Analysis of MRI-derived spleen iron in the UK Biobank identifies genetic variation linked to iron recycling and erythrocyte morphology

Elena P. Sorokin[1*‡], Nicolas Basty[2*], Brandon Whitcher[2], Yi Liu[1], Jimmy D. Bell[2], Robert L. Cohen[1], Madeleine Cule[1*], E. Louise Thomas[2*‡]

Author affiliations

[1] Calico Life Sciences LLC, South San Francisco, California, USA
[2]Research Centre for Optimal Health, School of Life Sciences, University of Westminster, London, UK

*These authors contributed equally

‡Corresponding authors. Correspondence and requests for materials should be addressed to l.thomas3@westminster.ac.uk and sorokin@calicolabs.com.

Abstract

Aging, and the pathogenesis of many common diseases, involves iron homeostasis. A key role in iron homeostasis is played by the spleen, which is the largest filter of the blood and performs iron reuptake from old or damaged erythrocytes. Despite this important role, spleen iron content has not been measured previously in a large, population-based cohort. In this study, we quantify spleen iron in 41,764 participants of the UK Biobank using magnetic resonance imaging (MRI). We find that epidemiologic and environmental factors such as increased age, higher red meat consumption and lower alcohol intake correlate with higher spleen iron. Through genome-wide association study, we identify genetic associations between spleen iron and common variation at seven loci, including in two hereditary spherocytosis (HS) genes, *ANK1* and *SPTA1*. HS-causing mutations in these genes are associated with lower reticulocyte volume and increased reticulocyte percentage, while our common alleles are associated with increased expression of *ANK1* and *SPTA1* in blood and with larger reticulocyte volume and reduced reticulocyte percentage. As genetic modifiers, these common alleles may explain mild spherocytosis phenotypes observed in some HS allele carriers. Further, we identify an association between spleen iron and *MS4A7*, which colocalizes with a quantitative trait locus for *MS4A7* alternative splicing in whole blood, and with monocyte count and fraction. Through quantification of spleen iron in a large human cohort, we extend our understanding of epidemiological and genetic factors associated with iron recycling and erythrocyte morphology.

Keywords: Spleen iron, UK Biobank, Magnetic Resonance Imaging, Imaging-derived phenotype, Human Iron Economy, Hereditary Spherocytosis, Genome-wide association study, Rare variant association study, Phenome-wide association study

Introduction

In recent years, human genetic cohorts have grown in scale and complexity, and have facilitated the discovery of risk factors for both disease diagnoses as well as clinically relevant biomarkers, particularly in urine and blood.[1–3] However, in most tissues, precision phenotyping has lagged behind genotyping, due to limitations in quantifying parameters of internal organs non-invasively and at scale. In the UK Biobank (UKBB), an abdominal imaging protocol combined with recent advances in machine learning has enabled high-throughput quantification of high-dimensional medical imaging data, yielding quantitative organ-level phenotypes.[4,5] Such phenotypes may improve statistical power to resolve subtypes of disease.[6]

Although the accumulation of spleen iron has been investigated in specific disease groups, there have been few studies in unascertained cohorts[7] at least partly due to limitations in detecting and quantifying low levels of tissue iron in non-overloaded populations.[8,9] Instead, most research has focussed on high risk populations such as beta-thalassemia major[10–14] sickle cell disease (SCD)[11,13,15] hereditary hemochromatosis (HH)[13], and liver disease.[16] In these conditions, pathologically increased iron deposition in the parenchymal cells in the liver, pancreas and heart cause tissue dysfunction and disease.[17] By contrast, hereditary spherocytosis has been linked to accumulation of iron in the spleen in a small study.[18] Accumulation of tissue iron has also been implicated in the pathogenesis of metabolic diseases of aging including insulin resistance, type-2 diabetes and nonalcoholic fatty liver disease, referred to as dysmetabolic iron overload syndrome.[19,20] Although some earlier reports suggested that spleen iron was of limited clinical relevance[21], these findings have led to more widespread interest in organ iron measurement.

Recent discoveries clarify the molecular processes involved in the body's iron economy, and offer a compelling framework to explore spleen iron in the general population. In normal physiology, the spleen plays a critical role in filtering and digesting old or damaged red blood cells. The splenic iron pool resides mainly in its macrophage population and appears to be highly dynamic, normally containing only about 50mg of iron while clearing and releasing back to plasma 20-25 mg/day. In contrast, intestinal absorption of iron is typically only 1-2mg per day. Both processes are understood to depend on the membrane protein ferroportin and the secreted hormone hepcidin. In the spleen, ferroportin facilitates the efficient transport of recycled iron from macrophages back into the plasma where it is bound by transferrin. Given the large iron flux through the normal spleen due to red cell recycling, measurement of spleen iron has the potential to reflect activity of iron salvage pathways.[22–24]

Spleen iron may also reflect red blood cell (RBC) health, including common hemolytic anemias that arise when RBC membrane structure is perturbed. For example, hereditary spherocytosis (HS) is a common red cell membrane disorder, occurring at a prevalence of 1:1000-2500 in European populations.[25] Patients have defects in a small set of membrane and cytoskeletal genes that contribute to RBC membrane integrity and deformability, including *SPTA1*, *ANK1*, *SPTB*, *SLC4A1*, and *EPB42.*[26] *SPTA1* encodes the filamentous protein alpha-spectrin, and *ANK1* encodes a protein that tethers spectrin filaments to red cell membranes.[27] The protein products of these genes physically interact in the formation of the mature RBC cytoskeleton, a process that accompanies the intense cellular remodeling occurring during reticulocytosis.[28]

In HS, the resulting RBCs tend to become spherically shaped and lose deformability quickly, and ultimately become trapped and ingested by splenic macrophages within the red pulp, resulting in an enlarged spleen and anemia despite brisk reticulocytosis. When measured directly with radiolabeled cells, RBC turnover is dramatically accelerated in patients with severe HS.[29] While laboratory measures such as mean sphered cell volume and mean reticulocyte volume can be used to accurately diagnose HS[30], less is understood about the phenotypic and genetic heterogeneity of the disease.[31–33]

To derive organ iron content measurements in a large and healthy population, non-invasive methods are needed. The UK Biobank (UKBB) is a prospective cohort study with genetic and phenotypic data from half a million adult participants in the United Kingdom.[34] In a subcohort of participants, phenotypic data includes Magnetic Resonance Imaging (MRI) imaging of the abdomen, including dedicated quantitative imaging of the liver.[4] Previously, we used deep learning and automated image processing techniques to quantify liver iron from liver acquisitions.[5] But depending on the size and position of the imaging slice, opportunistic measures of additional tissues within the field of view are theoretically possible.

In this study, we repurpose the MRI acquisitions of the liver to opportunistically measure spleen iron in the UKBB imaging subcohort, thus characterizing the distribution of spleen iron in a large, relatively healthy population for the first time. We confirm and extend observations from smaller studies that spleen iron varies by age, sex, ethnicity and diet. By associating spleen iron with common and rare genetic variation, we characterize associations with the human iron economy and the red blood cell (RBC) cytoskeleton, and point to a novel locus, *MS4A7*, with links to altered isoform expression and monocyte abundance. Intriguingly, associations near RBC cytoskeletal protein-encoding genes, *ANK1* and *SPTA1*, are also linked to increased mRNA expression in whole blood, and exhibit effects on reticulocyte and red cell parameters that are the opposite of the effects observed in a Mendelian hemolytic anemia. By combining radiology, machine learning, and genetics, this work underscores a trans-disciplinary effort to enable discovery in large human cohorts.

Results

Quantification of spleen iron in a large population-based cohort

Out of 44,265 participants in the UK Biobank (UKBB) with both Dixon neck-to-knee and liver single-slice MRI sequences, we were able to opportunistically measure median spleen iron concentration (referred to as spleen iron hereafter) in 41,764 participants (Methods and **Figure 1A,B**). The imaging subcohort had an average spleen iron of 0.92 (s.d. 0.29) mg/g compared to liver iron of 1.24 (s.d. 0.32) mg/g (**Table 1**). By quantifying organ iron from the same imaging acquisitions, we show that iron is significantly higher in the liver than in the spleen in a population-based cohort (**Figure 1C**; paired t-test $p < 2.2e\text{-}16$).

While there are are no accepted standards or specific cut-offs for 'normal' ranges of spleen iron, 1.98 mg/g (or R2* of $70s^{-1}$) has been suggested, with 2.74 mg/g (or R2* of $100s^{-1}$) reported to indicate pathological levels.[35] Using 1.98 mg/g as the criterion, 1.04% (n=435) of this cohort had elevated spleen iron, while 0.32% (n=137) of the cohort had spleen iron above

the 2.74 mg/g threshold. Additionally, 95% of the population fell into the range of 0.53 mg/g - 1.67 mg/g. We propose this as a possible reference range for spleen iron in an unselected population.

Spleen iron was associated with both age and sex. Males had on average 0.097 mg/g higher spleen iron than women (0.986 mg/g average for men vs 0.889 mg/g average for women) (p=6.3e-219; **Supplementary Table 2**). Increasing spleen iron content was associated with increasing age (0.0044 mg/g/year or 0.012 standard deviations/year) (**Figure 1D**). We found that menopause was associated with 0.12 mg/g [95% CI 0.08 - 0.16] higher spleen iron when adjusting for scan date and time and study center, but this was not independent of age. We tested whether menopause was associated with spleen iron above the 1.8 mg/g threshold but did not find a significant association (OR: 1.31 [95% CI 0.90 - 1.96] for post- versus pre-menopausal women; p=0.17). Taken together, age and sex are both important factors affecting spleen iron in a relatively healthy cohort not ascertained for iron disorders.

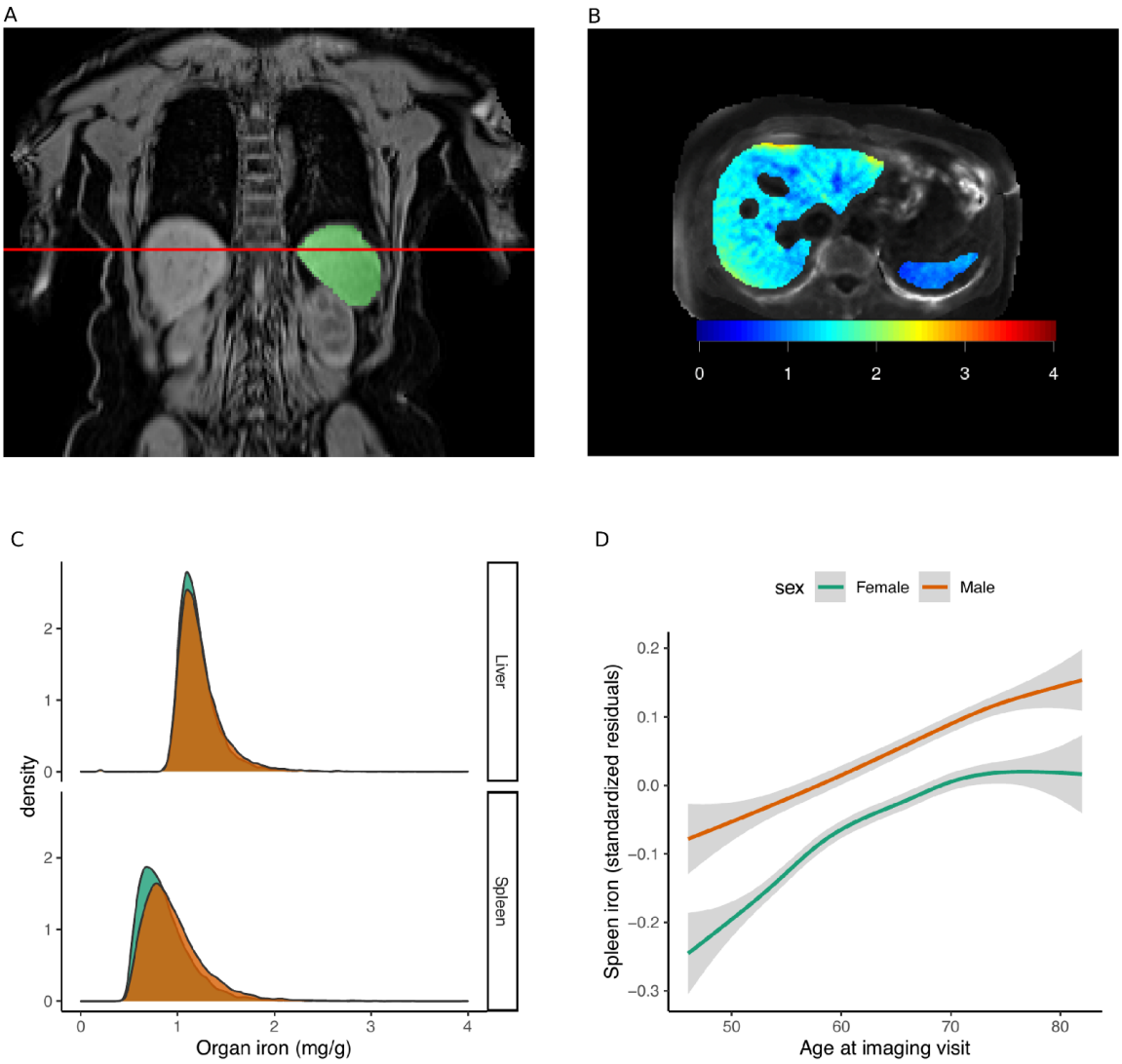

Figure 1: Image-based spleen iron measurement via opportunistic repurposing of the liver acquisition. A) Positioning of the liver slice (red line), with the neural network spleen

segmentation shown (green). **B)** Iron concentration (mg/g) for the liver and spleen. **C)** Distribution of organ iron in males and females. **D)** Spleen iron increases with age for both males and females. Standardized residuals are shown, adjusted for study center, scan date and scan time.

	UK Biobank cohort (at time of baseline visit)	Imaging cohort (at time of imaging visit)	Identified in combined liver slices	
			Liver	Spleen
n	502,520	44,265	44,265	41,764
% Female	54.4 [54.2-54.5]	51.8 [51.2-52.1]	51.8 [51.3-52.3]	52.1 [51.6-52.6]
Age	56.5 (8.1)	64.2 (7.73)	63.7 (7.56)	64.1 (7.71)
BMI (kg/m^2)	27.4 (4.8)	26.5 (4.37)	26.5 (4.39)	26.4 (4.32)
Height (cm)	168 (9.28)	169 (9.27)	169 (9.29)	169 (9.26)
% Caucasian	81.4 [81.3-81.5]	84.8 [84.4-85.1]	85.2 [84.4-85.5]	84.7 [84.4-85.0]
Iron concentration (mg/g)			1.24 (0.29) [0.203 - 6.96]	0.915 (0.318) [0.172 - 6.68]

Table 1: Summary of the UKBB cohort at recruitment, image acquisition, and quantification of liver iron and spleen iron. Spleen iron measurements (mg/g) are provided as mean (standard deviation) and range. For other quantitative values, the mean (standard deviation) is given. For binary values, mean [95% confidence interval] is given.

Spleen iron is associated with environmental factors, clinical outcomes, and serum biomarkers of iron stores

In a phenome-wide association study (PheWAS) of over 3,200 quantitative traits and disease outcomes, we identified a significant correlation between spleen iron and certain red blood cell parameters including reticulocyte percentage (beta=0.091; p=3.7e-66), reticulocyte count (beta=0.087; p=6.6e-64), and high light scatter reticulocyte count (beta=0.089; p=5.8e-64). Spleen iron was also positively associated with self-reported lifestyle factors, such as consumption of lamb (beta=0.150; p=2.1e-44), beef (beta=0.143; p=1.3e-43) and pork (beta=0.124; p=2.2e-31), and negatively associated with alcohol consumption (beta=-0.087; p=1.7e-18). Spleen iron correlated with iron content in the brain, specifically with T2* measures (inversely proportional to iron) in the caudate (beta=-0.063; p=4.3e-16) and putamen (beta=-0.061, p=4.1e-15).[36] Correlations between spleen iron and medical history and disease found associations across the disease phenome: with myeloid leukemia (beta=0.386; p=9.6e-10), chronic dermatitis (beta=0.328; p=4.1e-07), hypokalemia (beta =0.286, p=5.8e-6), glaucoma (beta=0.186, p=1.0e-6), and a negative association with vascular/heart problems (beta=-0.061, p=1.2e-6) and abdominal hernia (beta=-0.074,p=7.8e-5) (**Figure 2** and **Supplementary Tables 3 and 4**). Spleen iron was negatively correlated with

iron-deficiency anemia diagnosis, but the result was not significant (beta=-0.134, p=0.002), likely because this diagnosis is not well-captured by medical billing data (n=580 cases, n=35,316 controls).

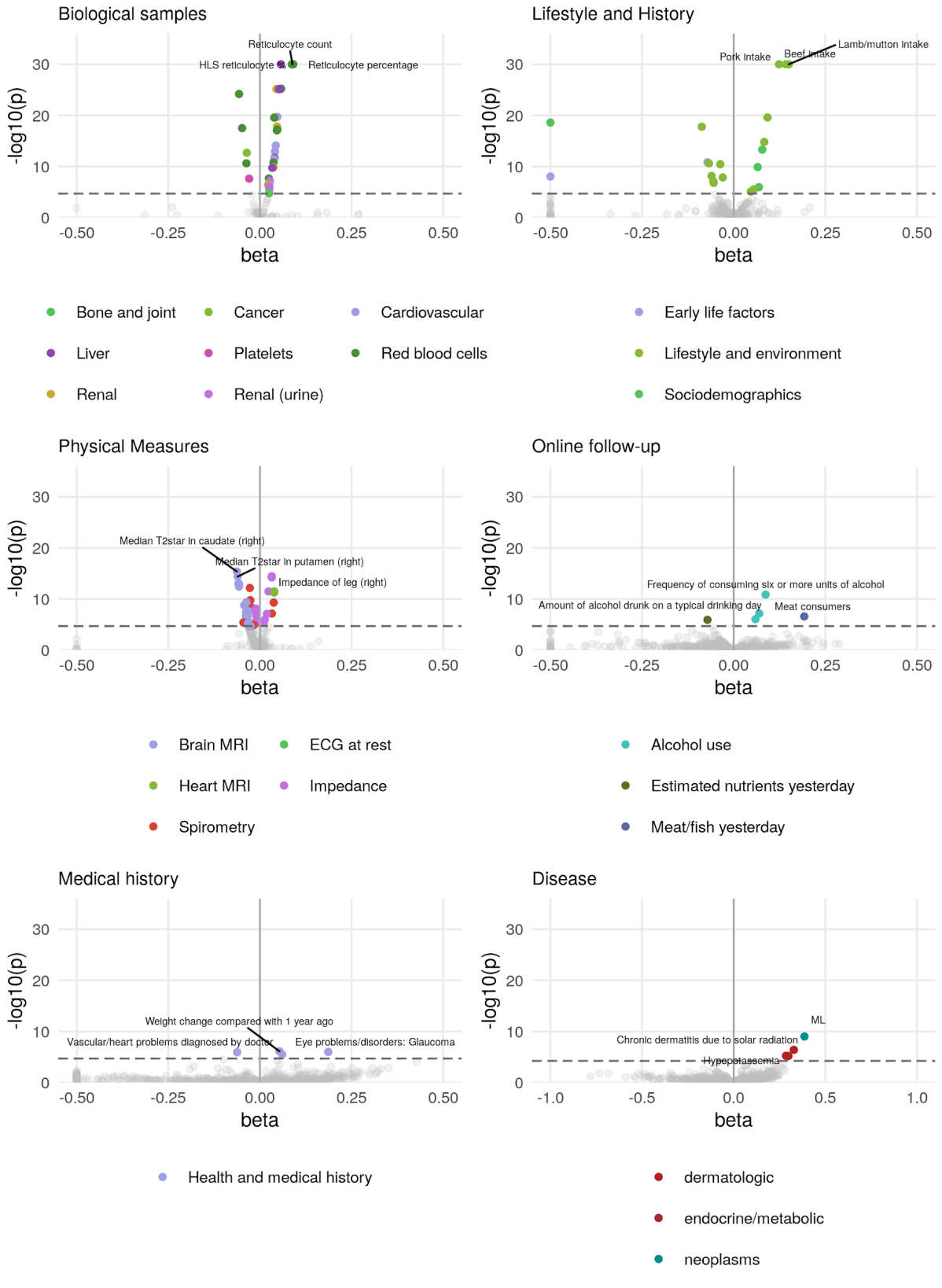

Figure 2: Phenome-wide association between spleen iron and other complex traits in the UK Biobank. The horizontal line shows a significant association after Bonferroni correction. The top three associations in each category are annotated. ML: Myeloid leukaemia. HLS reticulocyte: High light scatter reticulocyte.

In an analysis of genetic correlation with 288 complex traits including several relevant iron biomarkers[37,5] and red blood cell biomarkers (Methods), we identified genetic correlations with ferritin (r_g=0.56, p=1.1e-8), mean corpuscular hemoglobin concentration (r_g=0.42, p=2.6e-6), transferrin saturation (r_g=0.26, p=2.5e-3), liver iron (r_g=0.24, p=1.7e-2), a weak anticorrelation with total iron binding capacity (r_g=-0.20, p=1.9e-2), and no genetic correlation with pancreas iron (**Supplementary Tables 5 and 6).**

Genome-wide association study of spleen iron

To understand the contribution of genetic variation to variability in spleen iron, we studied the genetic architecture of this complex trait. First, we estimated the SNP heritability as 16.7% (s.e. 1.64%) using BOLT-REML (see Methods), indicating that spleen iron has a genetic component. Second, we conducted a genome-wide association study (GWAS) in a sample size of 35,324 (see Methods), and found that seven loci reached genome-wide significance ($p < 5e-8$; **Figure 3** and **Table 2**). Conditional analysis yielded no secondary signals at any of these loci.

We observed a signal on chromosome 2 at *SLC40A1*, which encodes ferroportin (lead SNP: rs13008848[G], beta=-0.057, p=2.9e-10, **Figure 4A**). In a statistical test for co-localization with prior studies of serum ferritin, serum iron, and liver iron[5,37], we observed evidence for regional co-localization with the lead spleen iron SNP at the ferroportin locus (posterior probability≥0.99) (**Supplementary Table 7**). Since our lead variant for spleen iron lies upstream of the open reading frame for ferroportin, we tested for a shared effect between spleen iron and *SLC40A1* expression across 56 tissues of the GTEx consortium.[38] We observed evidence for regional co-localization with a quantitative trait locus for *SLC40A1* mRNA in many tissues, including whole blood (posterior probability≥0.99), suggesting a potential regulatory mechanism by which variation in expression of *SLC40A1* may affect the human iron economy (**Figure 4D**; **Supplementary Table 8**).

Additional findings included a locus intronic to *KLHL29* on chromosome 2, and a locus on chromosome 9 (**Supplementary Figure 5B**). The lead SNP rs115697725[G] (beta=0.06, p=4.8e-8) in *KLHL29* co-localized with SNPs associated with mean corpuscular volume, mean corpuscular hemoglobin, mean reticulocyte volume, and mean sphered cell volume, as well as mRNA expression of *KLHL29* in multiple tissues (posterior probability≥0.99) (**Supplementary Table 9)**. This signal near *KLHL29* also co-localized with transferrin saturation and total iron binding capacity, but not ferritin or serum iron (**Supplementary Table 7**). By contrast, the lead SNP rs41276777[A] (beta=0.17, p=2.1e-9) occurred in the 5' untranslated region of *PRPF4* and *CDC26* (**Supplementary Figure 5A**). This SNP was associated with a regulatory locus affecting expression of both *PRPF4* and *CDC26* mRNA in multiple tissues, including whole blood and the spleen (**Supplementary Table 8**), suggesting bi-directional regulation of gene expression. This region colocalized with signals for serum ferritin, serum iron, and other blood iron traits (**Supplementary Table 7**), suggesting roles not only in spleen iron content but body iron content more broadly.

Both common and rare regulatory variation in genes encoding cytoskeletal structural proteins are associated with spleen iron and red blood cell traits

Two of the top associations from GWAS occurred in *SPTA1* and *ANK1,* which encode structural components of the red blood cell cytoskeleton (**Figure 4B-C; Supplementary Figure 6**). The lead SNP rs2479868[T] (beta=-0.083, p=2.5e-22) on chromosome 1 is located in an intron to *SPTA1*, and the lead SNP rs4737010[A] (beta=-0.077, p = 1.0e-17) on chromosome 8 lies intronic to *ANK1*. We tested for a shared signal with mRNA expression levels of *SPTA1* and *ANK1*, and observed co-localization with cis-regulatory variation for *ANK1* in multiple tissues (**Figure 4E-F**). Intriguingly, we noted that variation at each locus was associated with an increase in mRNA expression, as well as increased mean reticulocyte volume, decreased mean corpuscular hemoglobin concentration, decreased reticulocyte percentage, and decreased spleen volume (**Figure 5**). The magnitude and directionality for the changes in red cell parameters associated with the lead SNPs at *SPTA1* and *ANK1* were remarkably similar (**Figure 5**). In a regression model testing for interaction between the loci at *SPTA1* and *ANK1*, the interaction term estimate was not significant (beta=0.016, p=0.28), indicating that the effects at the two loci are independent of one another.

Using available summary data from the Blood Cell Consortium[39], we tested for replication of the associations and directions of effect between *SPTA1* and *ANK1* and mean corpuscular hemoglobin concentration and mean corpuscular volume in a cohort of European ancestry, and replicated our findings (p<5e-10 for all associations); additionally, we observed replication in cohorts of East Asian and Hispanic/Latino ancestry (p<0.05 for all associations). Only the associations with mean corpuscular hemoglobin concentration replicated in a cohort of African ancestry (p< 0.05 for both loci) (**Supplementary Table 10**).

Given the known associations of both *SPTA1* and *ANK1* gene defects with hereditary spherocytosis (HS), we performed an analysis of rare variation (minor allele frequency <0.0001) predicted to cause loss-of-function. Starting with 167,246 exomes of European ancestry, we conducted rare variant association studies for reticulocyte percentage and volume (see Methods) and identified one significant gene, *SPTA1*, in both studies (SKAT-O p-value < 1e-24; **Supplementary Figure 7**). Performing a scan of the same loss-of-function rare variation in *SPTA1* across the entire hematology panel, *SPTA1* was significantly associated with both increased reticulocyte percentage and increased mean corpuscular hemoglobin concentration, increased bilirubin, decreased mean sphered cell volume and decreased mean reticulocyte volume, thus recapitulating all of the clinical hallmarks of HS using putative deleterious alleles (**Supplementary Figure 7)**. We assessed whether this rare, deleterious variation was also associated with spleen iron, but did not observe any significant association in the imaging subcohort for either putative loss-of-function or deleterious missense variation, perhaps due to reduced statistical power of the imaging subcohort (n=18,420) compared to the exome cohort (n=167,246). (**Supplementary Figure 8**).

Finally, we genetically identified HS in the UKBB exome cohort using a combination of clinical assertions of pathogenicity as well as predicted high confidence loss-of-function in one of six genes, and estimated prevalence to be 1:389 [95% CI 1:427 - 1:354] (Methods). We asked whether the GWAS alleles could modify the effects of the rare deleterious alleles for any of the hematology parameters relevant for HS, including mean reticulocyte volume and reticulocyte percentage. We estimated that carrying either of the *SPTA1* or *ANK1* lead GWAS

SNPs skewed RBC parameters toward beneficial effects in deleterious allele carriers and non-carriers, suggesting that the common GWAS alleles could modify the effects of the rare deleterious alleles (**Supplementary Figure 10**).

Elevated spleen iron colocalizes with a splicing quantitative trait locus for CD20-like family member, *MS4A7*

We observed another significant association at the *MS4A7*/*MS4A14* locus (lead SNP: rs950802[A], beta=0.086, p=7.7e-26; **Table 2, Figure 6A**). The lead SNP causes a synonymous mutation at Leu57 in the third exon of *MS4A7* and is also a variant in the first intron of *MS4A14*. This signal colocalized with a signal from a recent study of serum ferritin levels[37]; posterior probability≥0.99). We asked whether expression of *MS4A7* or *MS4A14* co-localized with spleen iron at this locus, and observed co-localization for expression of both genes in many tissue types including whole blood (posterior probability≥0.99) (**Supplementary Table 8, Supplementary Figure 11**). Using splicing quantitative trait data[38], we identified an alternative splicing event in *MS4A7*, and colocalized it with spleen iron (**Figure 6B**). Based on an analysis of the open reading frame of *MS4A7,* this alternative splicing event is predicted to increase skipping of the second exon and therefore interrupt a conserved CD20-like transmembrane domain in *MS4A7* (**Figure 6C)**. We thus identify a novel association between *MS4A7* and spleen iron, and through fine-mapping and colocalization, we suggest a splicing mechanism by which this variant disrupts *MS4A7* function.

To further explore the functional consequences of regulatory variation in *MS4A7*, we examined its association with hematological parameters, and observed a significant association with monocyte count and percentage, as well as platelet count and platelet crit (**Figure 6D**). These findings are borne out by data in the Human Cell Atlas[40], indicating striking enrichment of *MS4A7* mRNA in monocytes compared to sixteen other hematopoietic cell types (**Figure 6E**). Moreover, we observed higher expression of *MS4A7* mRNA in the spleen relative to other tissues (**Figure 6F**). Taken together, we hypothesize that a novel common allele at the *MS4A7* locus is associated with elevated spleen iron, decreased mRNA expression of *MS4A7*, and an increase in monocyte fraction and absolute count, suggesting a potential role for this gene in regulating iron recycling in the spleen.

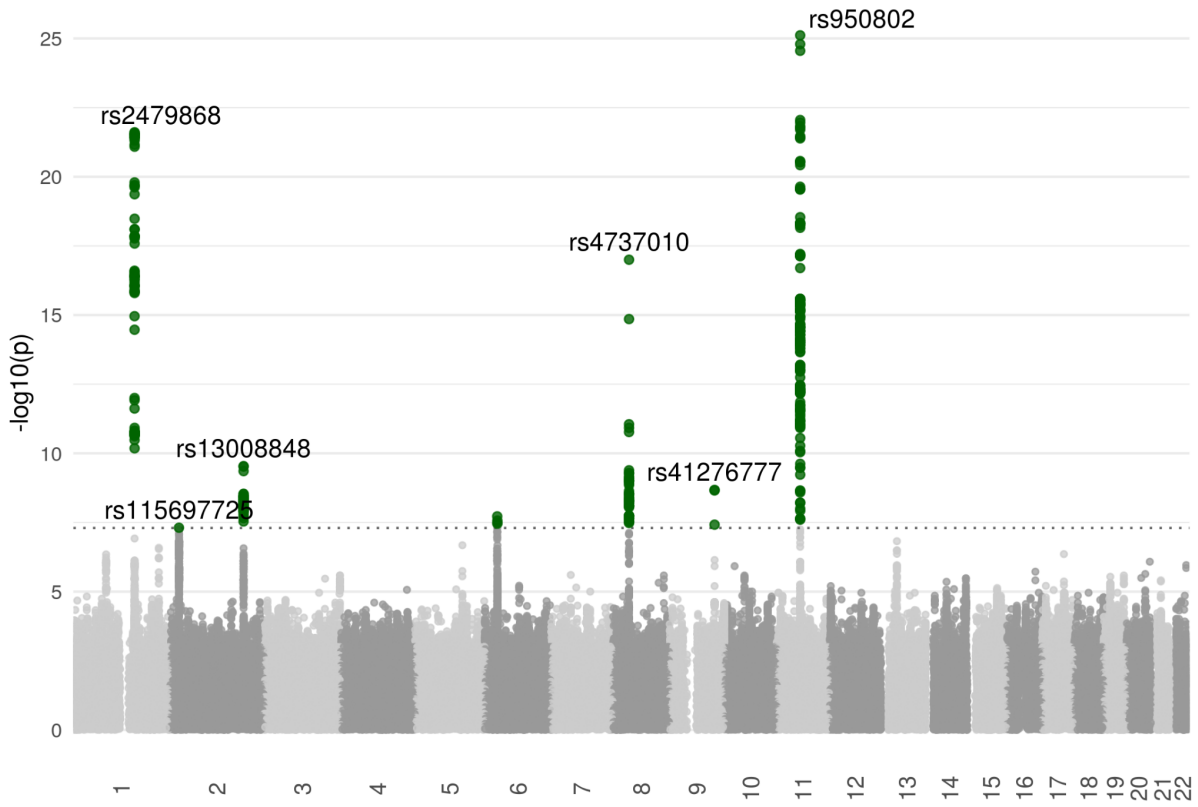

Figure 3. Genome-wide association study of spleen iron. Genome-wide significant signals (except the signal at the MHC locus on chromosome 6) are annotated with the variant at each locus. Dotted horizontal line marks genome-wide significance (p=5e-8).

Lead SNP	Locus	Lead SNP consequence	Effect Allele	Other Allele	Beta	p	Minor Allele Frequency
rs950802	*MS4A14*	Synonymous variant	A	G	0.086	7.7E-26	0.307
rs2479868	*SPTA1*	Intron variant	T	C	-0.083	2.5E-22	0.266
rs4737010	*ANK1*	Intron variant	A	G	-0.077	1.0E-17	0.228
rs13008848	*SLC40A1*	5 prime UTR variant	G	C	-0.057	2.9E-10	0.226
rs41276777	*PRPF4*	5 prime UTR variant	A	G	0.175	2.1E-09	0.019
rs115697725	*KLHL29*	Intron variant	G	C	0.059	4.9E-08	0.146

Table 2: Fine-mapped lead SNPs from genome-wide association study of spleen iron. Genome-wide significant associations (p<5e-8) are shown by locus and lead SNP after fine-mapping. A seventh association at the major histocompatibility locus (MHC) could not be fine-mapped.

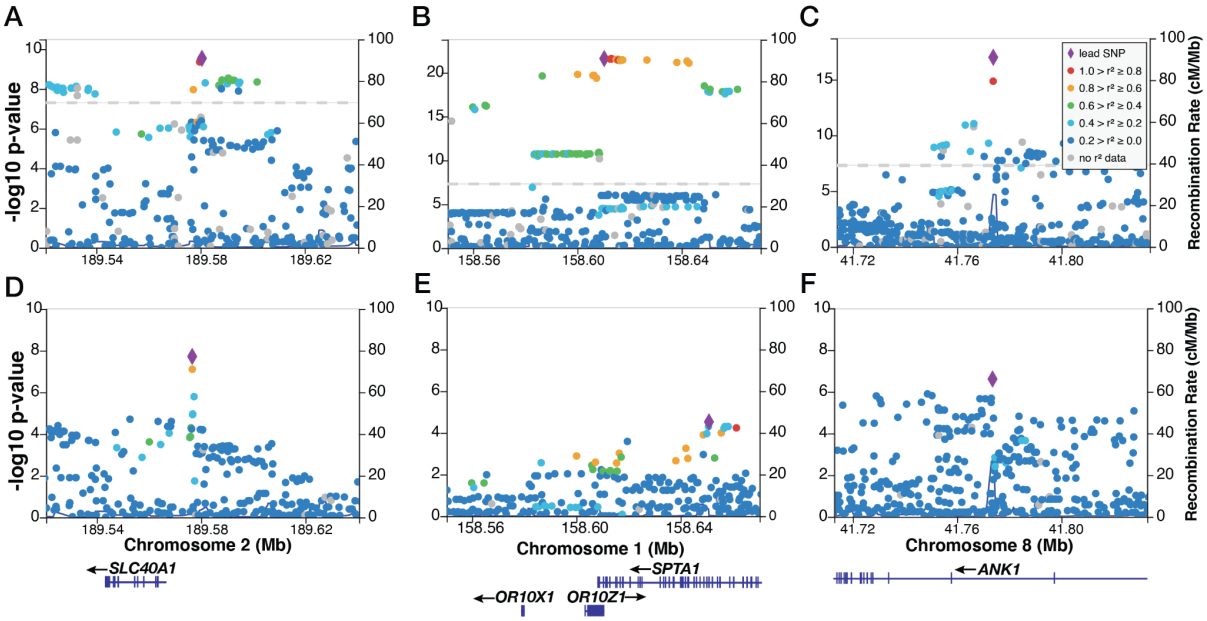

Figure 4: Common variants in *SLC40A1, SPTA1,* and *ANK1* loci are associated with spleen iron, and colocalize with cis-regulatory variation and blood biomarker traits. (A) Fine-mapped locus near *SLC40A1* is associated with spleen iron (lead SNP: rs13008848). **(B)** Fine-mapped genome-wide significant locus near *SPTA1* is associated with spleen iron (lead SNP rs2479868). **(C)** Fine-mapped locus near *ANK1* is associated with spleen iron (lead SNP: rs4373010). **(D)** Co-localization of cis-regulatory variation in the *SLC40A1* locus and spleen iron. Co-localization at this locus was observed in multiple tissues: blood, lung, and thyroid (posterior probability≥0.99 for each). Blood cis-eQTL data is shown. **(E)** Cis-regulatory variation in the *SPTA1* locus co-localizes with spleen iron. A signal was observed in multiple tissues but did not meet significance threshold in several tissues; for example, whole blood (posterior probability=0.719). **(F)** Cis-regulatory variation at the *ANK1* locus co-localizes with spleen iron. Co-localization was observed in multiple tissues (posterior probability≥0.99). Grey dashed line indicates genome-wide significance (p=5e-8). For eQTL signals, a threshold of FDR<5% was used[38]. Linkage disequilibrium was calculated using 1000 Genomes Phase 3. Gene models are shown at bottom in GRCh38 coordinates.

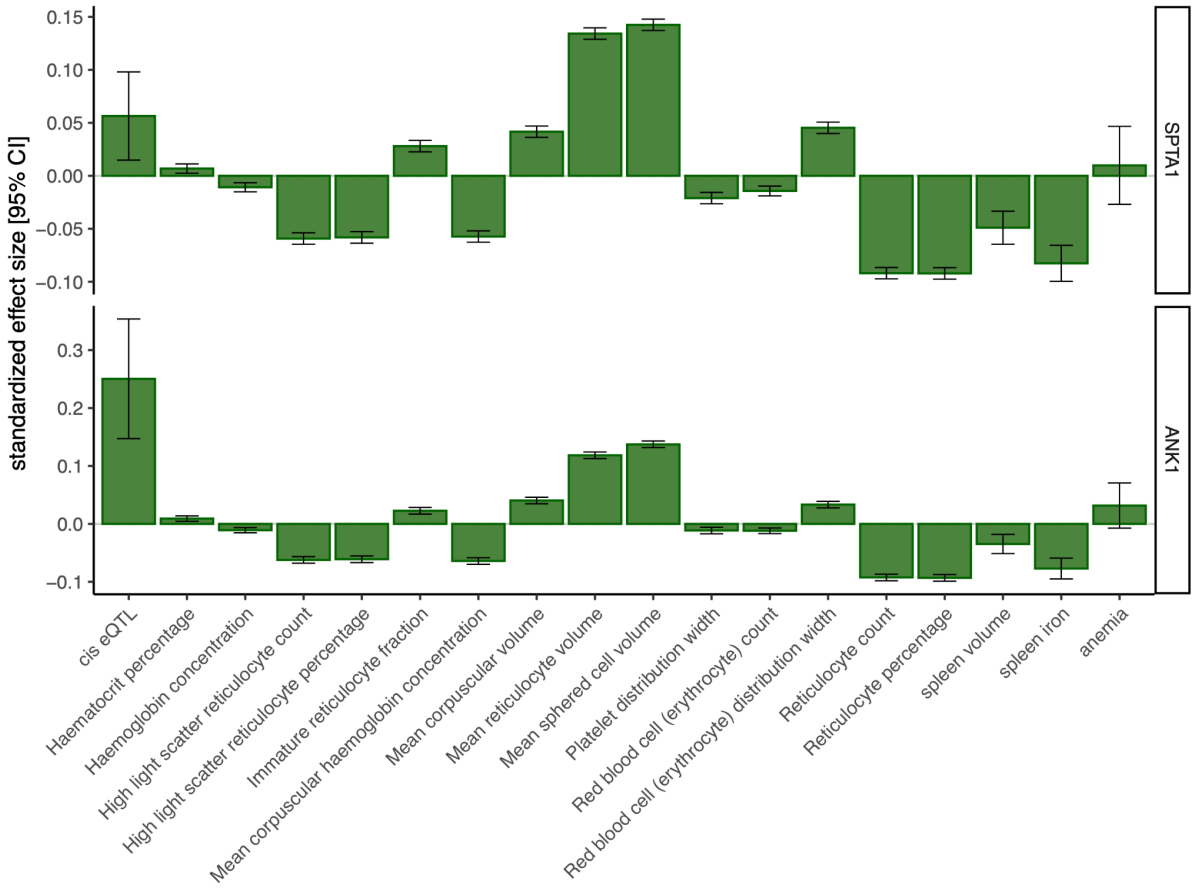

Figure 5: Associations of hematologic traits with lead SNPs at *SPTA1* and *ANK1* loci. Decreased spleen volume and mRNA expression were associated with rs4737010[A] at the *ANK1* locus and rs2479868[T] at the *SPTA1* locus. Relative changes in RBC and reticulocyte indices, expressed as standardized effect sizes, are shown.

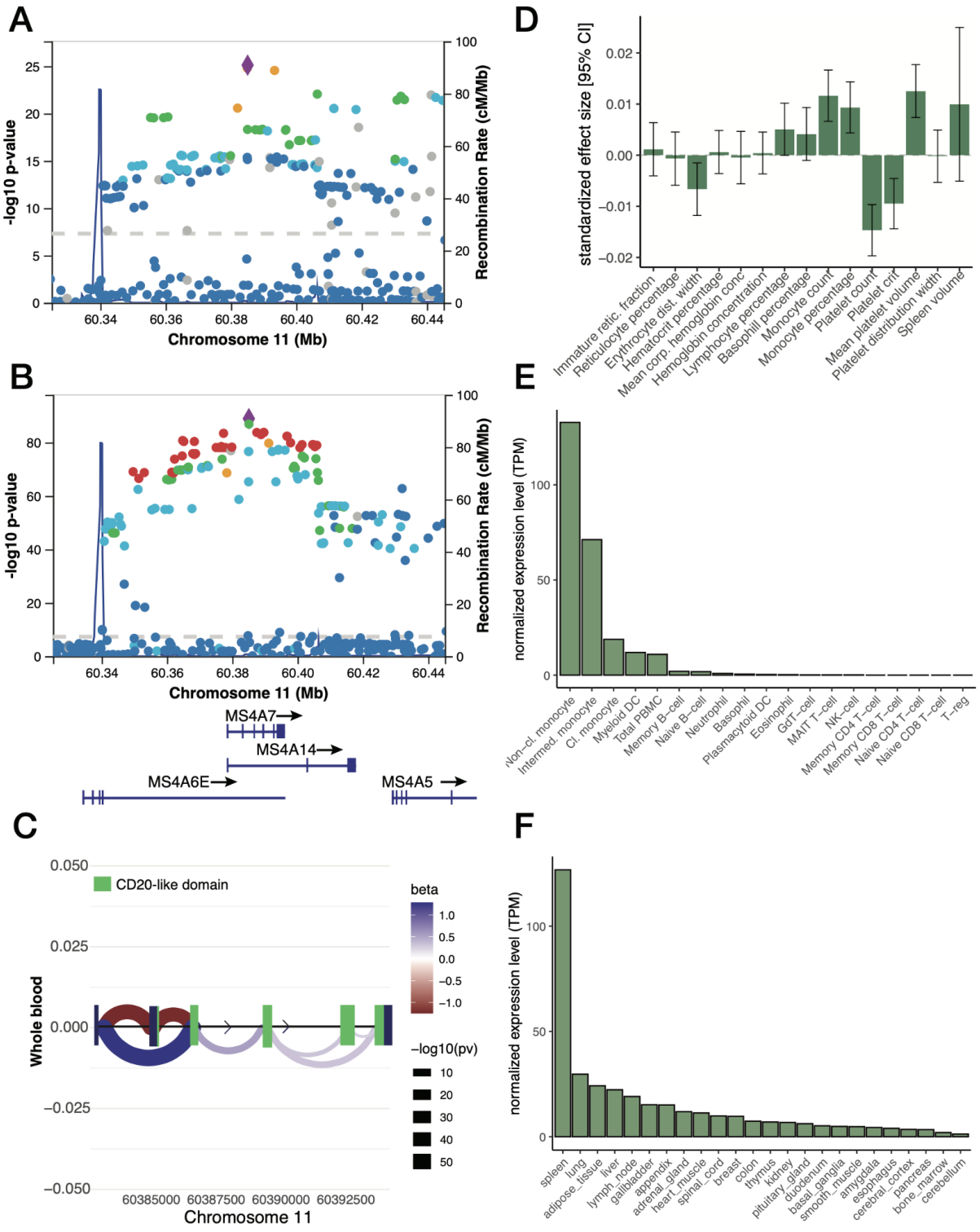

Figure 6: **Splicing regulation at the *MS4A7/MS4A14* locus is associated with spleen iron.** **(A)** The *MS4A7/MS4A14* locus on chromosome 11 is associated with an increase in spleen iron. Purple triangle displays the lead SNP rs950802[G] **(B)** This locus co-localizes with splicing quantitative trait locus (sQTL) of *MS4A7* in whole blood (posterior probability≥0.99). **(C)** Alternative splicing at the *MS4A7* locus as observed by the sQTL. The *MS4A7* gene model is displayed with the conserved CD20-like domain shown in green. **(D)** The *MS4A7* locus

displayed positive associations with monocyte count, monocyte percentage and mean platelet volume, and negative associations with platelet count and platelet crit. **(E)** Expression of *MS4A7* messenger RNA (mRNA) is enriched in monocytes, including non-classical, intermediate, and classical forms. **(F)** Expression of *MS4A7* mRNA in human tissues displays enrichment for lymphoid tissue, notably spleen and lymph nodes.

Discussion

In this study, we measured spleen iron concentration in 41,764 participants of the UK Biobank (UKBB) by repurposing specialized MRI acquisitions of the liver. MRI-derived values of spleen iron were generally consistent with previous estimates from extremely small cohorts.[7,41] Unlike the present study, most clinical studies have not included healthy volunteers, or used methods that cannot reliably assess iron content[11,42–44] or only provided qualitative histological grading.[44,45] Previously reported levels of spleen iron in disease are therefore highly variable, depending on aetiology, cohort age and MRI acquisition method employed (**Supplementary Table 11**).[10,13,14,16] Studies comparing MRI and chemical analysis of tissue could provide a more definitive cut-off, but this is unlikely to be feasible in healthy volunteer populations.

Spleen iron concentration is influenced by epidemiological and environmental factors, including sex, age and diet. For instance, spleen iron was higher in male subjects, consistent with prior reports in which the difference is attributed to the impact of the menstrual cycle on whole body iron stores in women.[46] Further, spleen iron increased with age (**Figure 1D**).[47] Spleen iron was associated with both red meat intake and inversely associated with alcohol consumption, extending prior findings of association between liver iron and these traits.[4849] Finally, we observed strong associations with red blood cell (RBC) parameters, including indicators of RBC turnover such as reticulocyte measures. As the spleen is the filter of RBCs in the blood, this strongly suggests that red cell turnover and reticulocytosis could be significant factors in the level of spleen iron.

We observed a modest correlation (pearson r=0.31 [95% CI 0.30-0.32]) between concentration of iron in the spleen and in the liver, which may in part reflect total body iron stores. In disease states, the nature of iron accumulation in different organs appears to depend on the aetiology of iron overload: in classical haemochromatosis, iron predominantly accumulates in the liver hepatocytes before affecting the heart and pancreas, while overload arising from transfusional hemosiderosis more commonly accumulates in the reticuloendothelial system affecting spleen, bone marrow and the Kupffer cells in the liver.[50] Literature reports differ regarding the relationship between accumulation of iron in the spleen and liver[11,16]: some have reported weak correlations[13], while others[7,12,14] reported stronger correlations in patients with **β**-Thalassemia, or diffuse liver disease.[16] A strong correlation was observed in patients with SCD, but not in controls or patients with non-transfusion dependent thalassemia.[51] Our study provides a first-of-a-kind comparison of iron concentration across organs using a large, relatively healthy, population-based cohort unascertained for anemias or iron overload.

Using spleen iron as an outcome for both genome-wide and rare variant association studies with whole exome sequencing data, we identified both common and rare alleles in two genes,

SPTA1 and *ANK1,* either of whose deficiency results in Hereditary Spherocytosis (HS), a hemolytic anemia. In our study, common variant signals in *SPTA1* and *ANK1* were associated with decreased spleen iron and colocalized with cis-acting expression quantitative trait loci (cis-eQTL). In addition to the observed cis-eQTLs in both the *SPTA1* and *ANK1*, the specific patterns of changes in RBC and reticulocyte parameters are strikingly similar, as both variants were associated with larger reticulocyte volume and mean cell volume, but all measures of reticulocyte production were decreased (**Figure 5**). Importantly, no association with anemia was noted for either common variant, suggesting that these are not pathologic variants. Since the spleen is the major route of RBC clearance and iron salvage, lower levels of reticulocytosis would be expected to result in lower spleen iron at steady state. A turnover-driven model would also predict that iron levels in other organs not involved in red cell clearance (e.g. pancreas) should be unaffected by these two loci, consistent with our observation that neither locus co-localized with any signals from GWAS of pancreas or liver iron. Our interpretation of these associations, based on known features of RBC and reticulocyte structure and dynamics, is that the decreased spleen iron resulted from low splenic turnover of relatively large long-lived red cells--the opposite phenotypic effect as is observed in HS patients.

In this study, we identify common variant genetic modifiers of rare deleterious alleles in *SPTA1* and *ANK1,* which may help to explain the variable penetrance and expressivity observed in HS patients. In a recent study of patients with identified HS mutations[31], 64% involved *SPTA1* or *ANK1,* and the investigators observed multiple HS families with broad phenotypic variability, including a compelling example of dizygotic twins sharing the same pathogenic *ANK1* mutation presenting with mild disease in one case and severe disease requiring splenectomy in the other. The variation could not be explained by genetic modifiers among the genes chosen for targeted sequencing, leading to speculation that yet-unknown genetic factors may be contributing. We were able to identify the hallmarks of HS using blood biomarker associations: we observed that loss-of-function variation in *SPTA1* was associated with increased reticulocyte percentage, increased mean corpuscular hemoglobin concentration, increased bilirubin, decreased mean sphered cell volume and decreased mean reticulocyte volume, all of which are in the opposite direction of effect as observed for the common *SPTA1* and *ANK1* variants (**Figure 5**, **Supplementary Figure 7)**. We therefore propose that the common variants identified here in *SPTA1* and *ANK1*, which are associated with increased mRNA expression, are protective modifiers of the HS phenotype. To further support this, we note that both loci deviated significantly from Hardy Weinberg equilibrium (p=9.0e-8 for *SPTA1* lead SNP, p=7.28e-17 for *ANK1* lead SNP), though a selection scan with phased haplotype data will be needed to determine whether these loci are under positive selection.

We characterized a polymorphism associated with decreased spleen iron at *SLC40A1*, encoding ferroportin, and showed via co-localization that this variant is also associated with increased expression of *SLC40A1* mRNA in several tissues sampled by the GTEx consortium,(**Figure 4D**). These observations are consistent with the role of ferroportin in the body's iron economy.[23] The cis-eQTL observed here may result in increased ferroportin expression in splenic macrophages and facilitate export of iron salvaged from senescent RBCs to the plasma. Although the steady-state spleen iron level detected by MRI associated with the common allele is low, iron appears to be efficiently recycled such that there is no association with RBC phenotypes or anemia. The phenotype observed here appears to be generally opposite to that described in Ferroportin Disease (FD), a mild disease state in which

ferroportin loss-of-function mutations impair iron release by macrophages, resulting in reduced iron release to serum transferrin, and iron overload detectable by MRI of the liver and spleen.[52] In contrast, the hyperactive ferroportin-mediated transport suggested by our results could be of clinical value, for example in the setting of chronic inflammation.

We also identified an association between spleen iron and the *MS4A7/MS4A14* locus, where the lead SNP was associated with increased spleen iron and co-localized with a splicing quantitative trait locus for *MS4A7* mRNA isoforms in multiple tissue types, including whole blood (**Figure 6**). *MS4A7* belongs to the CD20 family of membrane proteins, which are expressed within the hematopoietic lineage and are largely uncharacterized.[53,54] The lead SNP at this locus, rs22332423[A], is also associated with blood cell traits including increased monocyte absolute count and fraction. *MS4A7* mRNA is enriched in monocytes compared to other hematopoietic cell types and in the spleen compared to other somatic tissues. It is thus possible that excess circulating monocytes can be recruited to provide an expanded reservoir in the spleen, contributing to the body's iron economy in addition to splenic macrophages[55], and that this contributes to spleen iron. *MS4A7* thus presents a possible opportunity for therapeutic intervention to restore homeostasis in iron disorders.

Taken together, our genetic findings suggest that steady-state levels of spleen iron are sensitive to alterations in RBC structure affecting cell turnover, as well as alterations in iron transport by splenic macrophages. *SPTA1*, *ANK1,* and *SLC40A1* have functions and disease associations that are well-understood in this context, while other loci identified here (*KLH29, PRPF4, CDC26*) also show iron and RBC associations that are more cryptic at present. Our findings regarding *MS4A7* may potentially illuminate additional details of splenic RBC clearance mechanisms. For example, the specific functional roles played by macrophages and monocytes in the splenic red pulp remain incompletely understood.[55,29] Whether *MS4A7* directly affects splenic monocyte populations to alter spleen iron remains to be determined.

This study has some caveats worth mentioning. First, we do not know if there are regional variations in spleen iron concentration, since we used a single slice from each participant. Second, as the only study of its kind to quantify spleen iron in a large prospective human cohort, no replication cohort is available to confirm the associations with spleen iron reported here, though we are able to replicate our findings on blood cell traits. Third, while this is the largest population-based study to date on spleen iron, it relies upon a dataset of largely European ancestry. While we found limited evidence that spleen iron varies by ethnicity (**Supplementary Figures 3-4**), studies in large, diverse cohorts are still needed. Finally, follow-on experimental work in the hematopoietic lineage of a model organism, such as a mouse, will be needed to test directly the functional consequences of regulatory variation on both spleen iron accumulation and RBC parameters, and additional characterization of the molecular mechanism of *MS4A7* and its role in the body's iron economy.

In summary, we have demonstrated the feasibility of measuring spleen iron opportunistically in the context of liver image acquisitions, maximising use of the data at no extra cost to scanning or participant time. We confirmed and extended observations from smaller patient-focused studies and found that spleen iron varies by age, sex, ethnicity and diet. We have associated seven loci with spleen iron, and through fine-mapping and co-localization, identified three of them in or adjacent to genes previously characterized in hereditary blood

cell disorders and found new protective alleles that help to illuminate potential mechanisms of red cell turnover. We also found a novel signal associated with spleen iron and altered monocyte populations at the *MS4A7* locus, improving our understanding of this otherwise uncharacterized gene. This study highlights the utility of large imaging cohorts in elucidating the genetic basis of complex tissue traits.

Methods

Image Acquisition

We used the UK Biobank (UKBB) liver single-slice multi-echo MRI and the neck-to-knee Dixon MRI[4] in 44,265 subjects. For the first approximately 10,000 subjects, a gradient-echo (GRE) sequence was used, and subsequently an IDEAL[56] sequence was used (1,364 participants had both and contained the spleen). The liver slice covers the abdominal width generally including the spleen due to its position relative to the liver. **Figure 1** shows a coronal view of the neck-to-knee Dixon and the location of the liver 2D slice in red **(A)**, the estimated iron content for the liver and spleen in the multi-echo slice **(B)**.

Image Analysis

Image processing pipelines for the Dixon and multi-echo acquisitions and deep learning algorithms for image segmentation are described in Liu et al.[5] 2D masks of the spleen and the liver were extracted from the 3D segmentations based on the single-slice location and organ intersection[57] (**Figure 1A**). Direct liver 2D segmentations[5] were used for validation, and comparing the masks obtained directly with those from resampling (**Supplementary Figure 1)** showed a correlation of 0.98 for proton density fat fraction (PDFF) and 0.94 for R2*. We applied a one-pixel erosion and computed the median value within that mask. We excluded 2D masks from analysis that had < 1% of the organ volume in voxel number as well as those with less than 20 voxels. The number of participants with successful extractions in each organ is shown in **Table 1**. We transformed R2* to iron mg as previously described.[58,48] Thresholds for excess iron accumulation were taken from the literature as R2* values[35] and converted to mg using the same method:.

$$\text{iron} = 0.202 + 0.0254 \times R2^*$$

Using the 1,364 participants with both the IDEAL and GRE acquisitions, we compared the R2* and PDFF measurements (**Supplementary Figure 2**). Spleen PDFF in the GRE and IDEAL acquisitions were not correlated, supporting the idea that measurements of spleen PDFF via MRI are the result of noise reconstruction.[59] We therefore did not perform subsequent analysis on the PDFF measurements but included them for completeness as a negative result. Spleen R2* in the GRE and IDEAL acquisitions were strongly correlated (R^2=0.86).

To combine data from the GRE and IDEAL acquisitions, we first ranked the measurements within each modality. Where individuals had both measurements, we averaged the ranks. We then applied an inverse normal transformation and performed subsequent analyses using these residuals.

In order to report population-level iron concentration values while accounting for systematic differences between the acquisitions, for individuals with only GRE R2* measures, we applied a linear transformation. This transformation was derived by fitting a linear model to the 1,364 individuals with spleen R2* measurements for both IDEAL and GRE modalities:

$$R2^*_{IDEAL} = -1.276 + 1.2366 * R2^*_{GRE}$$

While measurement of spleen fat was possible with measured values ranging between 0 and 4.98% (**Supplementary Table 1**), close scrutiny of these measurements for n=1,364 subjects who had two different acquisitions covering the same anatomy indicate a level of background noise (**Supplementary Figure 2B**; R^2=0.01) leading us to agree with Hong et al.[59], that MRI measured spleen fat is at the level of background noise and cannot be meaningfully quantified. By contrast, spleen iron was reproducibly measured from both GRE and IDEAL (**Supplementary Figure 2A**; R^2=0.86). Therefore, we focused subsequent analyses on spleen iron.

Epidemiological modelling of spleen iron risk factors

Associations of spleen iron with age, genetic sex, and self-reported ethnicity were performed in R version 3.6.3. using the linear and logistic models for spleen iron as a quantitative or binary trait, respectively, after adjusting for covariates including imaging center, date and time.

Exome variant annotation

We performed annotation using VEPv100, LOFTEE[60], CADD[61] and ClinVar (https://www.ncbi.nlm.nih.gov/clinvar/, downloaded on September 27, 2020) with a custom pipeline to select variants meeting high-confidence loss-of-function criteria, further filtered for rare variants (defined as cohort-specific minor allele frequency <0.001), see Supplemental methods for QC. Of 13,907,497 total variants passing quality control, we subset 286,456 high-confidence, rare loss-of-function variants, 2,919,962 rare missense variants (CADD sore >=20), and 13,705 rare clinical pathogenic variants in 19,992 European ancestry samples for further analysis.

Rare variant regression study

We performed rare variant burden and SKAT testing as implemented in SAIGE-GENE, using a mixed-effects model.[62] A kinship matrix was built in SAIGE from a filtered set of 354,878 genotyped variants (r^2<0.2, minor allele frequency >0.05, Hardy-Weinberg p-value >1e-10, excluding known regions of long-range linkage disequilibrium). The linear mixed model regression equation was as follows:

$$y_i = \alpha + X_{1,i}\beta_1 + X_{2,i}\beta_2 + X_{3,i}\beta_3 + X_{4,i}\beta_4 + X_{5,i}\beta_5 + X_{6,i} + X_{7,i}\beta_7 + X_{8,i}\beta_8 + \sum_{j=1}^{5} PC_{ij}\beta_i + G_i\beta + b_i + \epsilon_i$$

In the model, y_i is inverse-rank normalized spleen iron, X_1 is age at imaging visit, X_2 is age^2, X_3 is chromosomally determined sex expressed as a binary indicator variable, X_4 and X_5 represent the categorical variable of study center as two dummy variables variables, X_7 is

standardized scan date, X_8 is standardized scan time, PC_j represents the first five principal components of European genetic ancestry, and G_i represents the allele counts (0,1,2) for q variants in each gene to test. We then performed SKAT and burden tests in SAIGE-GENE[62] and reported both the p-value from SKAT-O, which is a linear combination of burden and SKAT: $Q_{SKAT-O} = (1-\rho)Q_{SKAT} + \rho Q_{burden}$where ρ is estimated as previously described.[62] To inform directionality of effect, we reported the betas from the burden test. To avoid unstable results at low sample size, we calculated cumulative minor allele count and thresholded at >=5 minor alleles per gene, including singletons and doubletons. Genomic inflation factor was calculated using the gap package and summary statistics were visualized in R using the ggplot package.

Identification of clinical carriers of *HFE*, hemoglobin, and *G6PD* alleles

A version of ClinVar was downloaded on February 1, 2021, from https://ftp.ncbi.nlm.nih.gov/pub/clinvar/vcf_GRCh37/. Pathogenic, likely pathogenic, and pathogenic/likely pathogenic variants were selected with a level of evidence of either a single submission with criteria provided, multiple submitters agree, or reviewed by an expert panel (there are no variants in hemoglobin genes with a practice guideline). Genotypes were calculated using PLINK v1.90 and R 3.6.3 to assess compound genotypes.

Genome-wide association study

We conducted a GWAS study in n=35,324 participants with complete covariates, using methods previously described.[63] Briefly, we used UKBB imputed genotypes[34] version 3, excluding single nucleotide polymorphisms (SNPs) with minor allele frequency <1% and imputation quality <0.9. We excluded non-Caucasian participants, exhibiting sex chromosome aneuploidy, with a discrepancy between genetic and self-reported sex, heterozygosity and missingness outliers, and genotype call rate outliers.[34] 9,911,384 SNPs passed our QC thresholds and were included in the study. We used BOLT-LMM[64] v2.3.2 to conduct the genetic association study. We included age at imaging, age squared, sex, imaging centre, scan date and time, and genotyping batch as fixed-effect covariates, and genetic relatedness derived from genotyped SNPs as a random effect to control for population structure and relatedness, and normalized the outcome variable using inverse rank normalization. In the genetic association study, we found no evidence for global inflation of test statistics (λ_{gc}=1.035; LD score regression intercept 1.0269 [s.e. 0.0072])

Heritability estimates

We estimated the heritability of each trait using the restricted maximum likelihood method[65], as implemented in BOLT-LMM with the --reml option.

Genetic correlation

We computed genetic correlation using bivariate LDSC.[66] In this analysis, we computed the genetic correlation between spleen iron and 288 complex traits with a heritability of at least 5% from the Neale Lab http://www.nealelab.is/uk-biobank/, plus organ iron measurements[5], and blood iron biomarkers.[37] We used a Bonferroni-corrected p-value threshold of 0.05/282=0.000177 to identify statistically significant genetic correlations.

Statistical fine-mapping and credible set construction

We performed approximate conditional analysis using GCTA[67], considering all variants within 500kb of the locus index variant. As a reference panel for LD calculations, we used genotypes from 5,000 UKBB participants[34] that were randomly selected after filtering for unrelated European ancestry participants. We excluded the major histocompatibility complex (MHC) region due to the complexity of LD structure at this locus (GRCh37::6:28,477,797-33,448,354; see https://www.ncbi.nlm.nih.gov/grc/human/regions/MHC). For each locus, we considered variants with locus-wide evidence of association (p-valuejoint<10−6) to be conditionally independent. We followed an iterative procedure to determine credible sets of causal variants with 95% coverage.[63]

Colocalization with gene expression and complex traits

For gene expression colocalizations, we used summary statistics from GTEx[68] v7. For disease and quantitative trait colocalizations, we used UKBB summary statistics of PheCodes[69], normalized quantitative traits (http://www.nealelab.is/blog/2017/7/19/rapid-gwas-of-thousands-of-phenotypes-for-337000-samples-in-the-uk-biobank). For analysis we selected UKBB phenotypes where the minimum p-value within the +-500kb region around the locus tag SNP was <5x10-8.

We performed colocalization analysis using the coloc R package[70] using default priors and all variants within 500kb of the index variant. We considered two genetic signals to have strong evidence of colocalization if PP3+PP4≥0.99 and PP4/PP3≥5 (**Supplementary Table 4**).[71]

Phenome-wide association study

Disease traits

We used the R package PheWAS[72] to combine ICD10 codes (Field 41270) into distinct diseases or traits (PheCodes). The raw ICD10 codes were grouped into 1,283 PheCodes, of which 885 had more than 20 cases and were included in the PheWas (**Supplementary Table 3**). For each IDP-PheCode pair, we performed a logistic regression adjusted for age, sex, height, and BMI, and imaging center, date, scan time, and self-reported ethnicity.

Other traits

We used the R package PHESANT[73] to generate an initial list of variables derived from raw data. We manually curated this list to remove variables related to procedural metrics (e.g., measurement date, time and duration; sample volume and quality), duplicates (e.g., data collected separately on a small number of participants during the pilot), and raw measures (e.g., individual components of the fluid intelligence score). This resulted in 1,824 traits (**Supplementary Table 2**). For each trait, we performed linear (quantitative traits) or logistic regression (binary traits) on the abdominal IDP, including imaging center, date, scan time, age, sex, BMI, and height, and ethnicity as covariates.

Replication analysis

Summary statistics from the Blood Cell Consortium[39] were downloaded from http://www.mhi-humangenetics.org/en/resources/ and harmonized using dbSNP build 151 (GRCh37). We tested for replication of rs2479867[T] in *SPTA1* and rs4737010[A] in *ANK1* using all available genetic ancestries: Europeans, East Asians, African-Americans, and Hispanic/Latinos in studies of mean corpuscular hemoglobin concentration and mean corpuscular volume.

Acknowledgments

We thank Marcia Paddock, Kevin Wright, and Amoolya Singh for helpful feedback and discussion. This research has been conducted using the UKBB Resource under Application Number 44584 and was funded by Calico Life Sciences LLC.

Author Contributions

NB, MC, EPS, JDB, ELT designed the study. NB, BW, and YL implemented the image processing methods. MC performed the data processing. EPS and MC performed genetic analysis. ELT, EPS, RLC, MC and NB drafted the manuscript. All authors edited, read, and approved the manuscript.

Declaration of interests

EPS, RLC and MC are employees of Calico Life Sciences LLC. YL is a former employee of Calico Life Sciences LLC. NB, BW, JDB, and ELT have no competing interests.

Data Availability

Model weights for spleen segmentation are available via Github (www.github.com/calico-ukbb-mri-sseg) and code for resampling at www.github.com/recoh/pipeline. All summary statistics will be made available from the GWAS Catalog (www.ebi.ac.uk/gwas) upon publication. All derived data will be made available from the UK Biobank (www.ukbiobank.ac.uk).

Figure Legends

Figure 1: Image-based spleen iron measurement via opportunistic repurposing of the liver acquisition. A) Positioning of the liver slice (red line), with the neural network spleen segmentation shown (green). **B)** Iron concentration (mg/g) for the liver and spleen. **C)** Distribution of organ iron in males and females. **D)** Spleen iron increases with age for both males and females. Standardized residuals are shown, adjusted for study center, scan date and scan time.

Figure 2: Phenome-wide association between spleen iron and other complex traits in the UK Biobank. The horizontal line shows a significant association after Bonferroni correction. The top three associations in each category are annotated. ML: Myeloid leukaemia. HLS reticulocyte: High light scatter reticulocyte.

Figure 3. Genome-wide association study of spleen iron. Genome-wide significant signals (except the signal at the MHC locus on Chromosome 6) are annotated with the variant at each locus. Dotted horizontal line marks genome-wide significance (p=5e-8).

Figure 4: Common variants in *SLC40A1, SPTA1,* and *ANK1* loci are associated with spleen iron, and colocalize with cis-regulatory variation and blood biomarker traits. (A) Fine-mapped locus near *SLC40A1* is associated with spleen iron (lead SNP: rs13008848). **(B)** Fine-mapped genome-wide significant locus near *SPTA1* is associated with spleen iron (lead SNP rs2479868). **(C)** Fine-mapped locus near *ANK1* is associated with spleen iron (lead SNP: rs4373010). **(D)** Co-localization of cis-regulatory variation in the *SLC40A1* locus and spleen iron. Co-localization at this locus was observed in multiple tissues: blood, lung, and thyroid (posterior probability≥0.99 for each). Blood cis-eQTL data is shown. **(E)** Cis-regulatory variation in the *SPTA1* locus co-localizes with spleen iron. A signal was observed in multiple tissues but did not meet significance threshold in several tissues; for example, whole blood (posterior probability=0.719). **(F)** Cis-regulatory variation at the *ANK1* locus co-localizes with spleen iron. Co-localization was observed in multiple tissues (posterior probability≥0.99). Grey dashed line indicates genome-wide significance (p=5e-8). For eQTL signals, a threshold of FDR<5% was used[38]. Linkage disequilibrium was calculated using 1000 Genomes Phase 3. Gene models are shown at bottom in GRCh38 coordinates.

Figure 5: Associations of hematologic traits with lead SNPs at *SPTA1* and *ANK1* loci. Decreased spleen volume and mRNA expression were associated with rs4737010[A] at the *ANK1* locus and rs2479868[T] at the *SPTA1* locus. Relative changes in RBC and reticulocyte indices, expressed as standardized effect sizes, are shown.

Figure 6: **Splicing regulation at the *MS4A7/MS4A14* locus is associated with spleen iron. (A)** The *MS4A7/MS4A14* locus on chromosome 11 is associated with an increase in spleen iron. Purple triangle displays the lead SNP rs950802[G] **(B)** This locus co-localizes with splicing quantitative trait locus (sQTL) of *MS4A7* in whole blood (posterior probability=0.99). **(C)** Alternative splicing at the *MS4A7* locus as observed by the sQTL. The *MS4A7* gene model is displayed with the conserved CD20-like domain shown in green. **(D)** The *MS4A7* locus displayed positive associations with monocyte count, monocyte percentage and mean platelet volume, and negative associations with platelet count and platelet crit. **(E)** Expression of *MS4A7* messenger RNA (mRNA) is enriched in monocytes, including non-classical, intermediate, and classical forms. **(F)** Expression of *MS4A7* mRNA in human tissues displays enrichment for lymphoid tissue, notably spleen and lymph nodes.

Supplementary information

Supplementary methods

Identification of GRE acquisitions with high iron content

Through the quality control process, it has come to our attention that the GRE echo times in the UKBB abdominal MRI protocol are not short enough to quantify iron when it is exceeding a threshold (approximately 4 mg/g). High iron concentrations have a superparamagnetic effect that distorts the local magnetic field resulting in a faster decay of transverse magnetization.[50] Values beyond this threshold are not detected in GRE and would be falsely assigned a low value unless flagged up. However, this issue may be accurately identified from the magnitude data across echo times. Using the 2D organ segmentations, we calculated the average signal intensity for each echo time. When the decay of these values had a drastic signal dropoff and the average values of the longest echo time magnitude images displayed no decay, we estimated that the iron is mischaracterized. We assigned a maximum iron value of 4 mg/g to those participants.

Quality Control/Assurance Methods

Exome sequence quality control

We performed quality control of n=200,643 whole exomes from the UKBB using our custom "FE-plus" pipeline. Raw genotype calls were filtered genotype-level quality metrics to identify quality outliers for a given site, and remove poor-quality individual-level genotypes. Similarly to the FE pipeline[74], we removed genotypes below a minimum read depth (for SNPs: 7 and for indels: 10), and genotypes below a minimum Phred-scaled genotype quality of 20. We removed genotypes where minor allele allelic balance < 0.15 for SNPs and 0.2 for indels. Supplementing FE filters with additional filters, we performed per-SNP QC, requiring the average genotype quality to be at least 30 and per-SNP depth of coverage to be at least 15, to filter out badly captured sites. Additionally, we removed variants with genotype missingness > 10% or that deviated meaningfully from Hardy Weinberg equilibrium in a European ancestry cohort (HWE p< 1e-10). Of 17,981,897 total variants, 13,907,865 variants passed QC in the European exome cohort with MRI data (n=18,240).

Filtering self-reported ancestry for outliers

Self-reported ethnicity continental ancestry (European, South Asian, African, and East Asian) was obtained from the UKBB (field 21000) and principal component analysis performed using common (minor allele frequency >=0.05), independent (r^2<0.2), autosomal markers, in Hardy Weinberg equilibrium (p>1e-10), excluding regions of long-range linkage disequilibrium. FlashPCA v2.1 was used to calculate the first 10 principal components (PCs). Centroid distance was calculated by subtracting the population PC mean from the individual's PC,

squaring, and dividing by the variance for that PC. Ancestry outliers were identified as extreme values on a histogram of centroid distance for PCs 1-3.

Genetic identification of hereditary spherocytosis alleles

From the exome cohort filtered for European ancestry (n=167,246), we annotated variants by clinical assertion as pathogenic according to ClinVar, downloaded from https://ftp.ncbi.nlm.nih.gov/pub/clinvar/ on September 27, 2020, and called predicted loss-of-function alleles using LOFTEE[60]). HS alleles were defined as clinical pathogenic variants or high-confidence putative loss-of-function alleles in one of six genes (*SPTA1, SPTB, SLC4A1, ANK1, EPB41,* or *EPB42).*

Supplementary results

Spleen iron varies by ethnicity

Spleen iron varied by self-reported ethnicity, even after pruning ancestry outliers and adjusting for age, sex, study center, scan date, and time ($p_{Kruskal\text{-}Wallis}$=2.1e-20; Methods, **Supplementary Figure 4**). Even after removal of the British group (n=32,414) which was considerably larger than the other groups, there were differences in group means ($p_{Kruskal\text{-}Wallis}$=1.1e-17). We performed a similar analysis using liver iron, adjusted for the same covariates, and observed differences in group means ($p_{Kruskal\text{-}Wallis}$=2.1e-4; **Supplementary Figure 4**). We note that the non-European groups were of small sample size in this study, and larger sample sizes are needed to confirm these observations.

HFE carriers and compound heterozygotes have elevated spleen iron as compared with non-carriers

HH is a recessive Mendelian disorder characterized by accumulation of iron in the liver, blood and other tissues and is most commonly caused by missense variants in the *HFE* gene, which regulates iron uptake into hepatocytes in the liver. We examined two missense variants, HFEp.Cys282Tyr and HFEp.His63Asp, both of which segregate in the UKBB at high frequency (HFEp.Cys282Tyr: minor allele frequency (MAF) = 0.146 [95% CI 0.145 - 0.146] HFEp.His63Asp: MAF = 0.073 [95% CI 0.073 - .074]). While we observed elevated liver iron in C282Y and H63D carriers, compound heterozygotes, and homozygotes (**Supplementary Figure 9A**), we did not observe any effects of HH carrier status on spleen iron, after adjustment for covariates (**Supplementary Figure 9B**).

Thalassemia is a blood disorder characterized by low levels of hemoglobin. Although there was only one participant with a confirmed diagnosis in the imaging cohort, we identified putative carriers of mutations in globin genes characterized as pathogenic or likely pathogenic in ClinVar. We detected 345 mutations in globin genes (*HBA, HBB, HBC, HBD, HBE, HBF, HBH,* and *HBS*) asserted as pathogenic or likely pathogenic in ClinVar. Of those, only three variants in HBA and 20 variants in *HBB* segregated within the entire UKBB. All of these

segregating variants were extremely rare, with the most common variant being rs33946267[C] in HBB, with a minor allele frequency of MAF=3.2e-4 in the entire UKBB. None of these carriers overlapped with the imaging cohort, precluding further analysis of thalassemia carriers.

Glucose-6-phosphate dehydrogenase (G6PD) deficiency is a genetic metabolic abnormality particularly in males, caused by deficiency of the enzyme encoded by *G6PD* which is associated with RBC dysfunction. We identified 15 pathogenic variants underlying G6PD deficiency. Here, three variants did segregate in the imaging subcohort, most commonly rs1050828[C], with a minor allele frequency of 1.2e-3. Within the imaging cohort, there were 19 males with one of three *G6PD* pathogenic mutations. We compared spleen iron in *G6PD* carriers to non-carriers in males, but did not observe a significant difference at this sample size (**Supplementary Figure 5**).

Supplementary Tables

Supplementary Table 1: Values for spleen and liver iron, PDFF, and R2* divided into GRE and IDEAL acquisitions in the UK Biobank.

Supplementary Table 2: Spleen iron concentrations in the UK Biobank, stratified by males and females.

Supplementary Table 3: Results from phenome-wide association study of spleen iron with 2,346 traits including medical history, lifestyle factors, and self-reported questionnaires.

Supplementary Table 4: Results form phenome-wide association study of spleen iron with 857 disease diagnosis codes.

Supplementary Table 5: Genetic correlations between spleen iron and 288 traits in the UK Biobank.

Supplementary Table 6: Genetic correlations between spleen iron and six previously published blood and organ iron traits: ferritin, serum iron, transferrin saturation (TSAT), and total iron binding capacity (TIBC)[37], and pancreas and liver iron[5].

Supplementary Table 7: Colocalization test results for genome-wide significant loci from the spleen iron GWAS with loci from six previously published blood and organ iron traits.

Supplementary Table 8: Colocalization test results for genome-wide significant loci from the spleen iron GWAS with expression quantitative trait loci (eQTLs) from 56 tissues of the GTex consortium (version 8).

Supplementary Table 9: Colocalization test results from genome-wide significant loci from the spleen iron study with hematological assays.

Supplementary Table 10: Replication analysis of *SPTA1* and *ANK1* associations with red cell parameters in an independent cohort of the Blood Cell Consortium, representing East Asian, African-American, Hispanic/Latino and European populations.

Supplementary Table 11. Comparative data from spleen iron measured by MRI in healthy volunteers and patient groups. T2* published values were converted into R2* values using the equation R2* = 1000/T2*. R2* published values were converted into [FE} in mg/g[58]. *Mean age only provided for mixed cohort, ↟Mean values calculated from individual patient values provided in the publication. MRI measurement of spleen iron may be expressed as signal intensity ratio based on T2w or T2*w imaging, T2, R2, T2* or R2*[42] or converted into values in mg/g using formulas derived from liver studies[58,75]. Older methods using changes in T2 relaxation are not as sensitive for mild or moderate spleen iron overload.[44] The upper range of T2* measures are higher than those measured using R2*, limiting direct comparison[43], furthermore, the relationship between R2 and R2* is different in the liver and spleen therefore R2 measurements may underestimate spleen iron[11], as such, they have not been included in this comparison.

Supplementary Figures

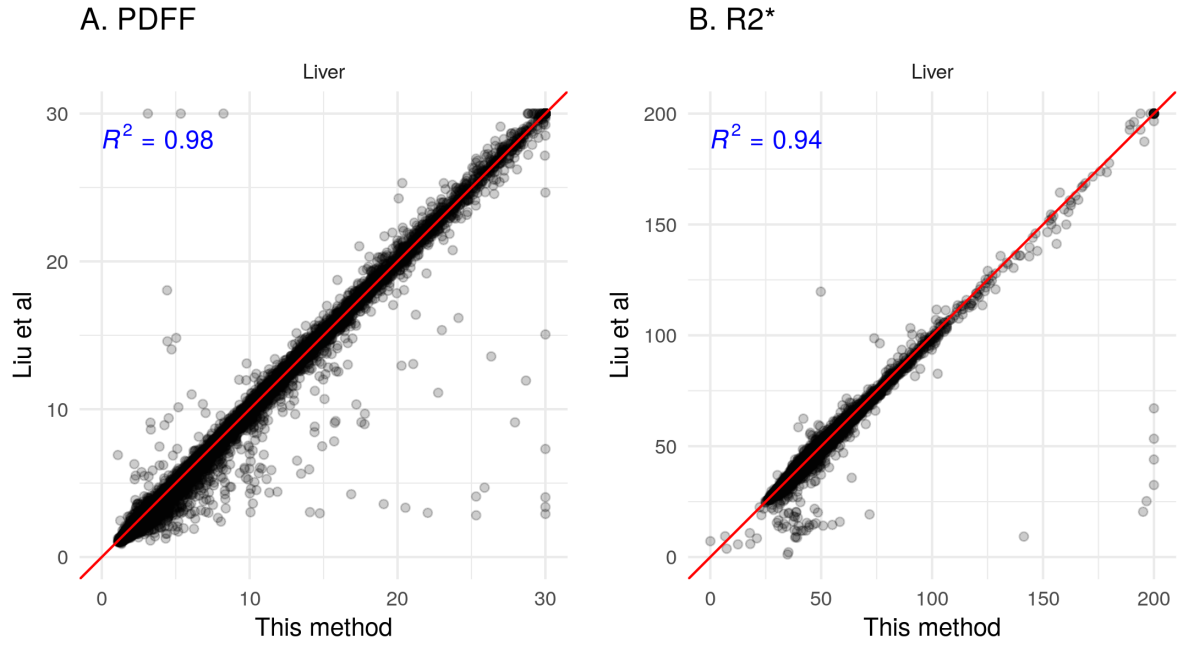

Supplementary Figure 1: Scatter plot comparing direct neural network-based segmentation[5] in a dedicated 2D slice (y-axis) with opportunistic resampling[57] from the 3D (Dixon) acquisition (x-axis) A) median liver PDFF (in %) and (B) median liver R2* (in s^{-1}) (n=38,400).

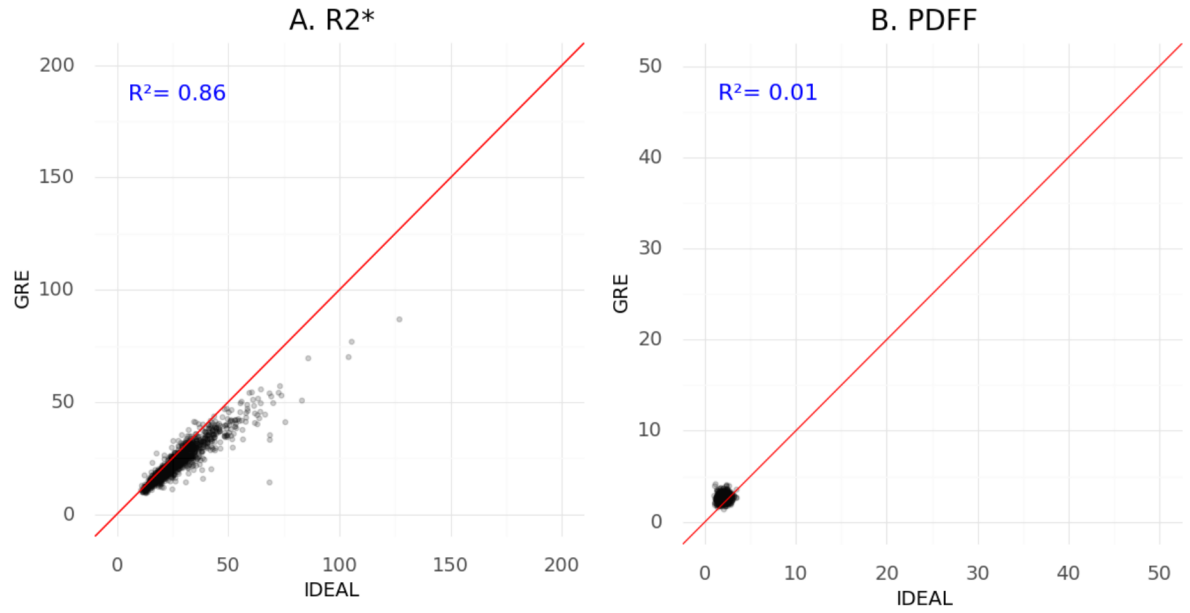

Supplementary Figure 2. Relationship between parameters measured in the spleen in n=1,364 UKBB subjects with both GRE and IDEAL single-slice multi-echo acquisitions. Scatter plots for median R2* (A) measurements (in s^{-1}) and PDFF in % (B). Pearson's correlation between the measures is given in blue.

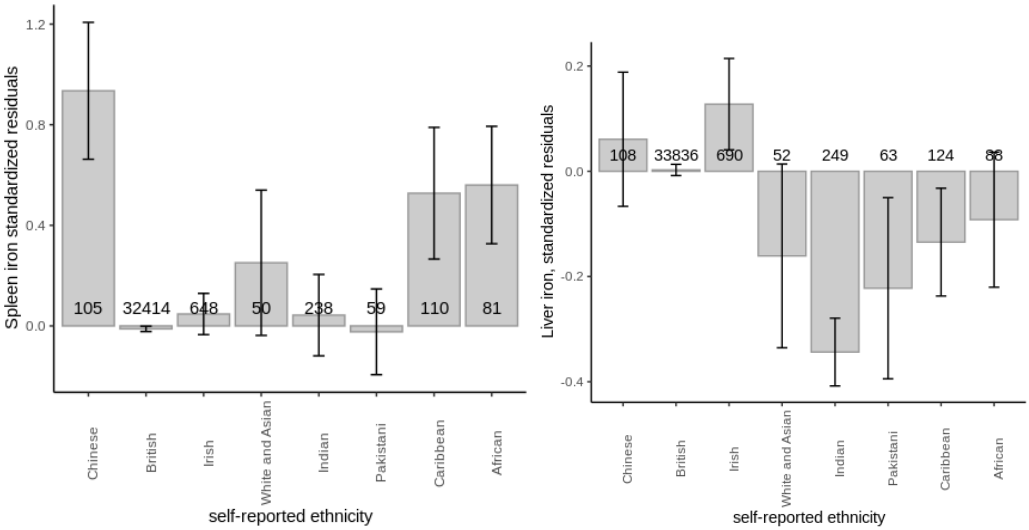

Supplementary Figure 3: Spleen iron varies by self-reported ethnicity. (A) Spleen iron displayed as standardized residuals after adjustment for age, sex, study center, scan date and time. (B) Liver iron content displayed as standardized residuals after adjustment for the same covariates. Only groups with >50 individuals with imaging phenotypes are shown. 95% CIs are shown.

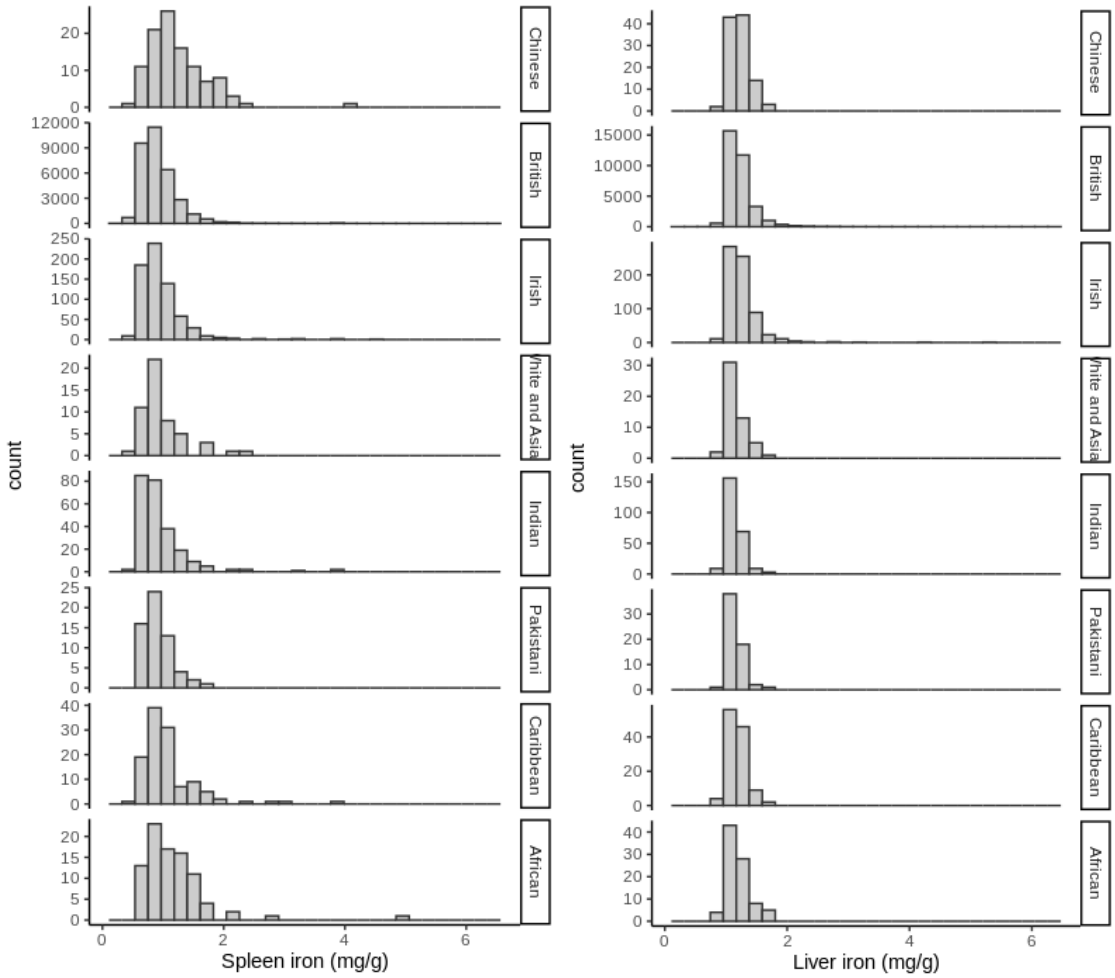

Supplementary Figure 4: **Spleen iron (in mg/g) varies by self-reported ethnicity but with a limited sample size for non-European groups**. Left panel: Histogram of spleen iron in mg/g by self-report ethnicity. Right panel: Histogram of liver iron content in mg/g by self-report ethnicity.

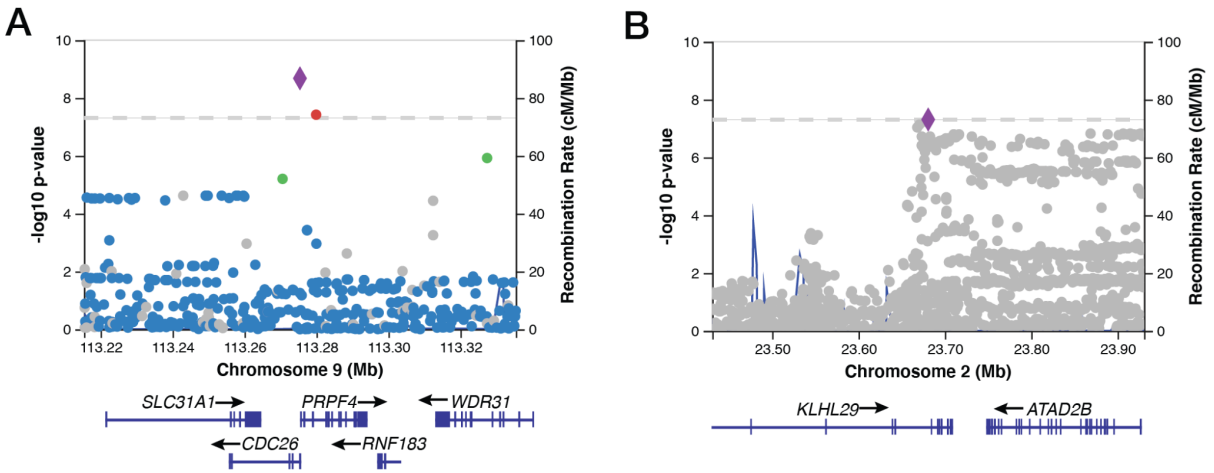

Supplementary Figure 5: Lead SNPs associated with spleen iron in the *PRPF4/CDC26* and *KLHL29* loci after statistical fine-mapping. (A) The lead SNP in the *PRPF4/CDC26* locus on chromosome 9 is rs41276777[A]. (B) The lead SNP in the *KLHL29* locus on chromosome 2 is rs115697725[G].

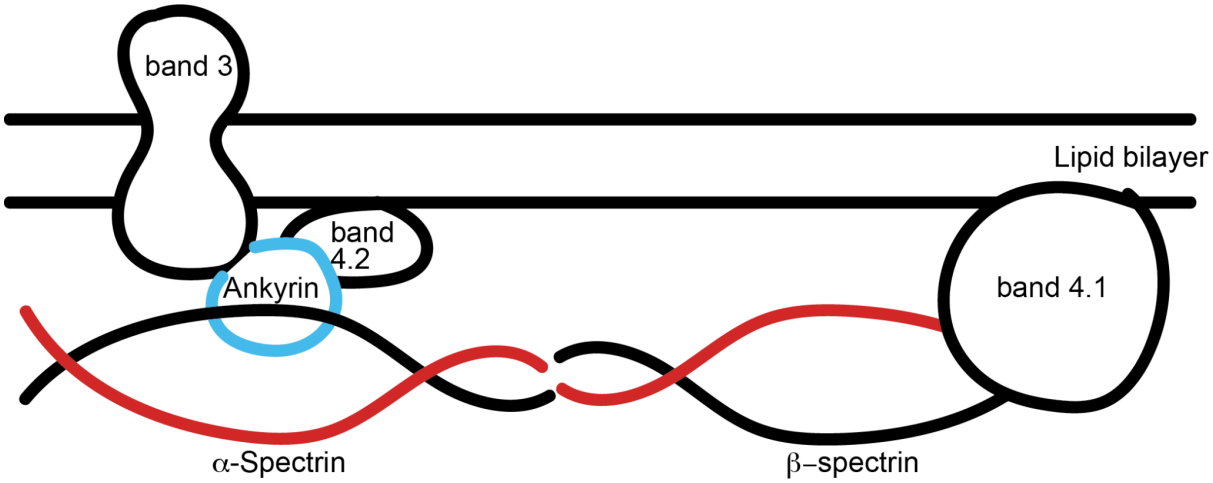

Supplementary Figure 6: Simplified cartoon of a cross-section of an red blood cell membrane cytoskeleton. Cytoskeletal protein ankyrin (encoded by the *ANK1* gene) is shown in blue, and alpha-spectrin (encoded by *SPTA1*) is shown in red. Alpha and beta spectrins contain antin-binding domains and associate to form anti-parallel heterodimers which interact to form tetramers. Ankyrins anchor anion exchangers in the lipid bilayer to the spectrin filaments. The anion exchanger band 3, as well as cytoskeletal proteins band 4.1, and band 4.2, are depicted for reference. Adapted from Delaunay et al.[26]

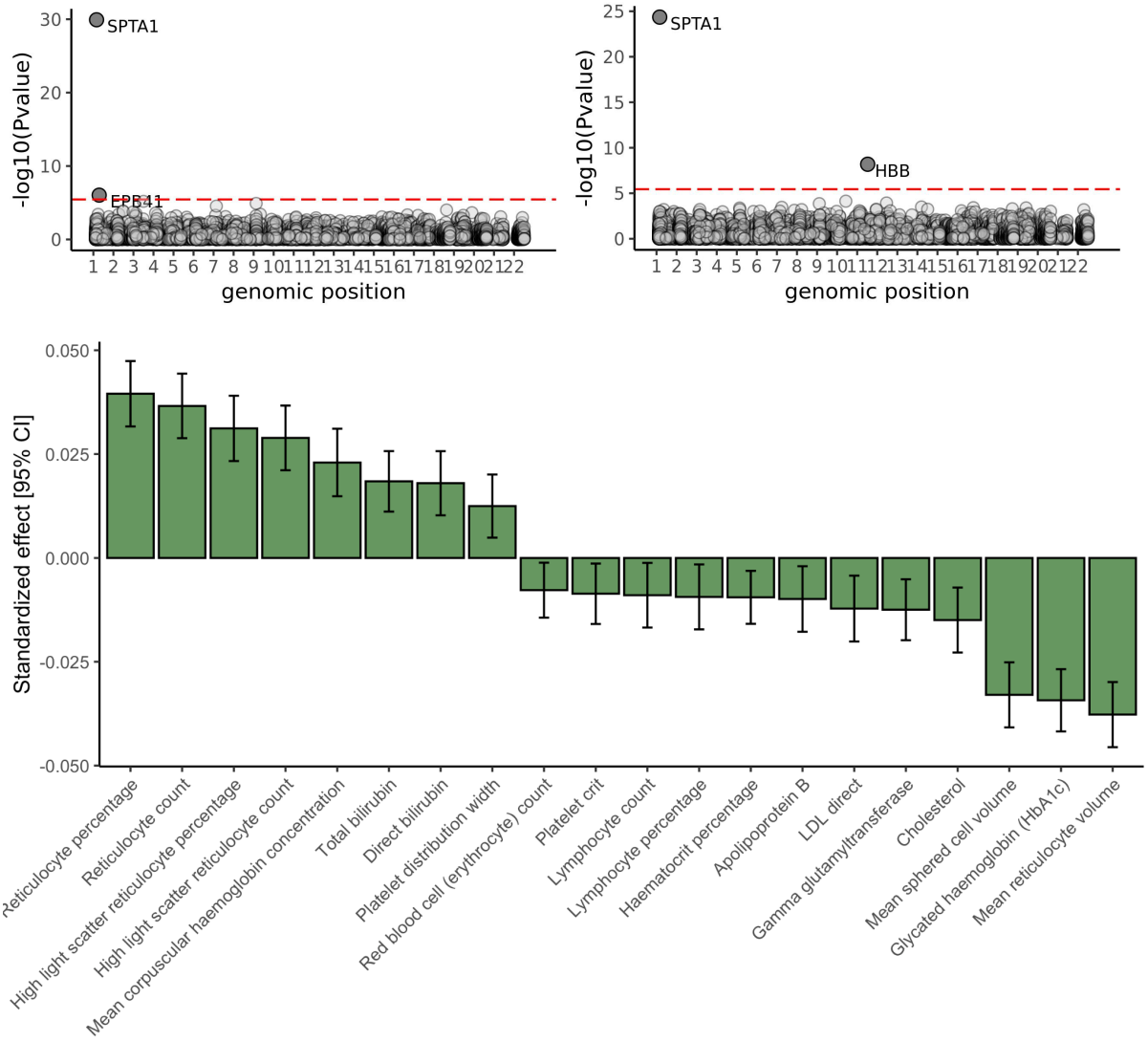

Supplementary Figure 7: Ultra-rare, predicted loss-of-function variation in *SPTA1* is associated with RBC biomarkers, platelet biomarkers, bilirubin, cholesterol, and glycated hemoglobin (HbA1c) in 167,243 exomes via rare variant association study (RVAS). Top left: Exome-wide association study (ExWAS) of reticulocyte percentage identifies two components of red blood cell membrane architecture: *SPTA1* (encoding alpha-spectrin) and *EPB41* (encoding band 4.1). **Top right:** ExWAS of mean reticulocyte volume identifies *SPTA1* and *HBB*, encoding beta hemoglobin Bonferroni significance is shown with the dashed red line. **Bottom:** ExWAS across a panel of 31 quantitative hematological traits for rare coding mutations in *SPTA1* recapitulated signatures of hereditary spherocytosis (HS), including increased reticulocyte percentage, mean corpuscular hemoglobin concentration, bilirubin; and decreased mean sphered cell volume and mean reticulocyte volume.

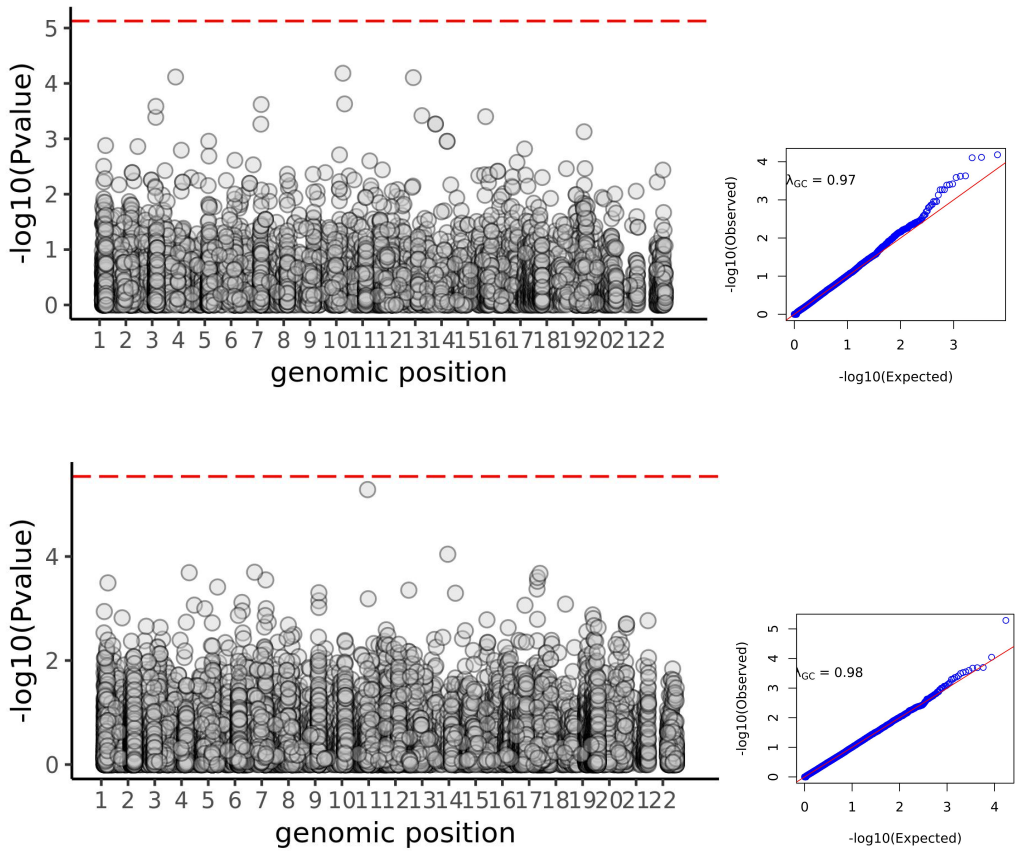

Supplementary Figure 8: Rare variant burden testing to identify associations with spleen iron. **Top panel:** Rare variant burden testing of loss-of-function variation in 18,240 exomes. 286,546 variants in 6,686 genes (minor allele count >=5) were tested. QQ plot is shown at right. **Bottom panel:** Rare variant burden testing of predicted deleterious missense variation. 2,919,962 variants in 17,298 genes (minor allele count >=5) were tested. QQ plot is shown at right.

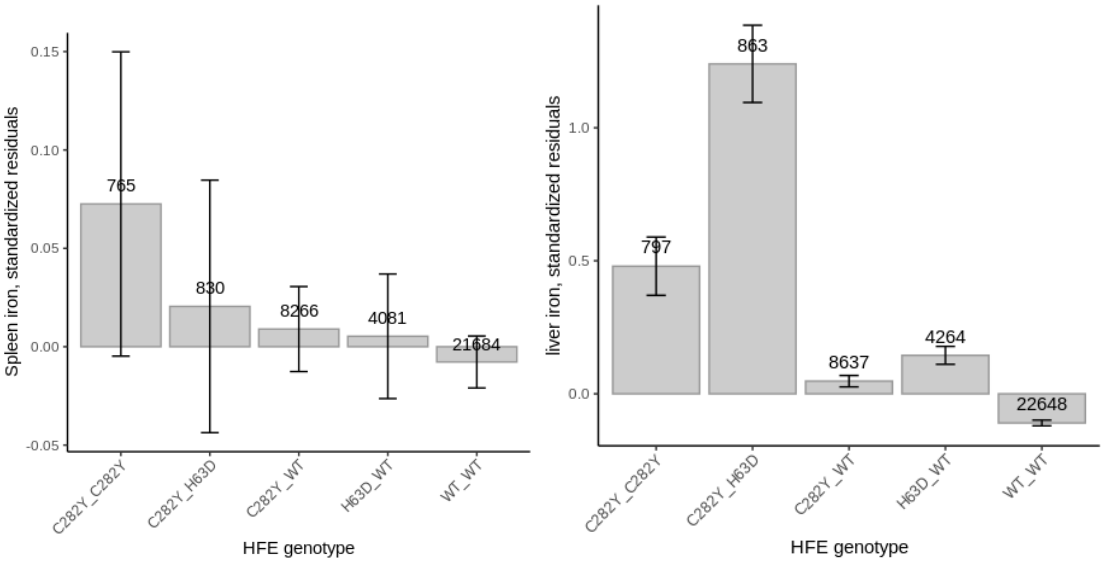

Supplementary Figure 9: Spleen iron in *HFE* carriers, homozygotes, compound heterozygotes and non-carriers. (A) *HFE*p.Cys282Tyr homozygosity, *HFE*p.Cys282Tyr/p.His63Asp compound heterozygosity, and *HFE*p.Cys282Tyr carrier status are not associated with significant differences in spleen iron. Standardized residuals of liver iron content, following adjustment for age, genetic sex, study center, scan date and time (B) Carrier status at the *HFE* locus affects liver iron. Standardized residuals of spleen iron, following adjustment for age, genetic sex, study center, scan date and time.

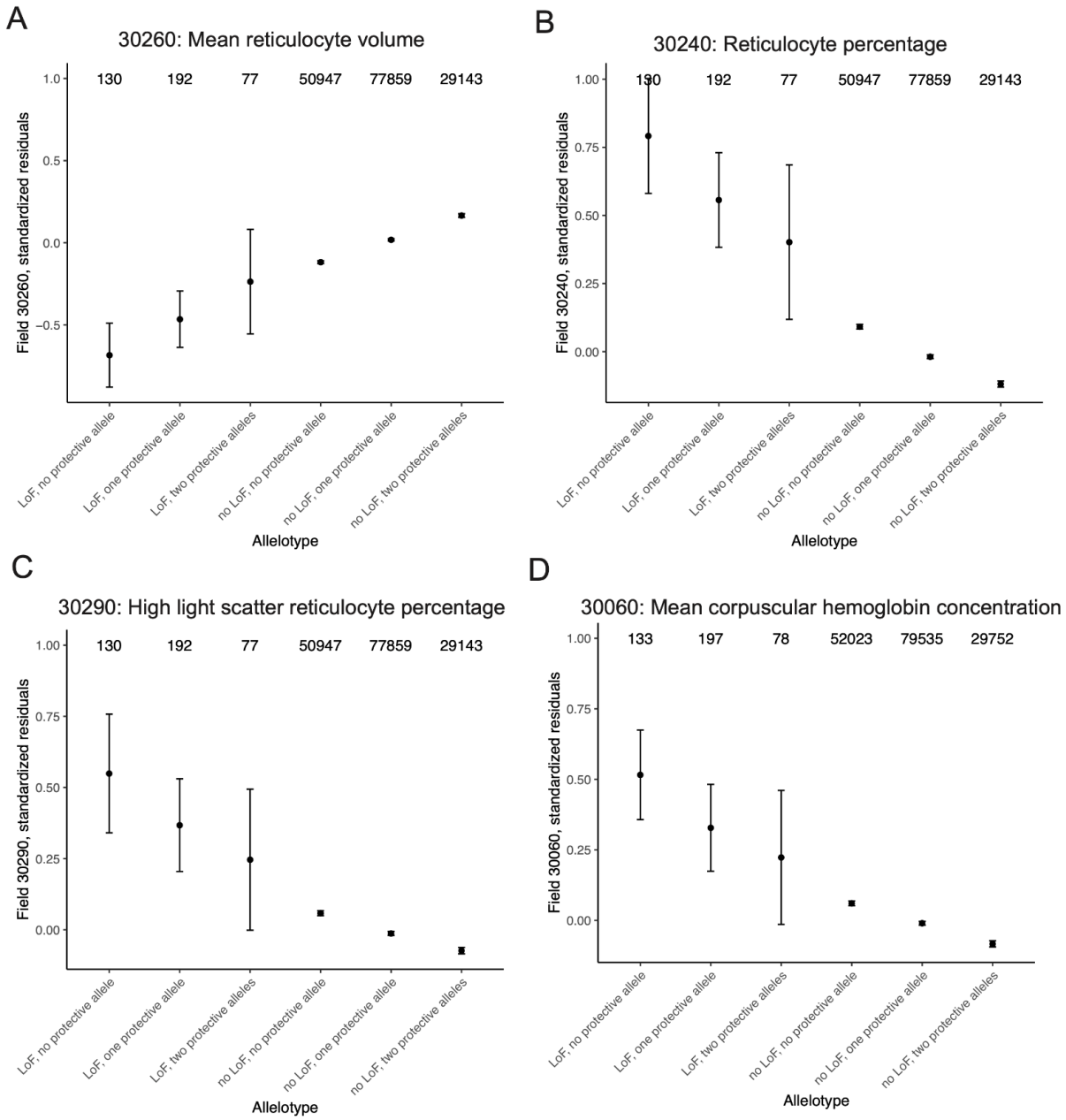

Supplementary Figure 10: Allelotype analysis comparing individuals with and without the common, 'protective' alleles in *SPTA1* or *ANK1*, and with and without putative deleterious

alleles in one of six hereditary spherocytosis (HS) genes. Standardized residuals, adjusted for age, sex, and global principal components of ancestry are shown for four red blood cell parameters: (A) mean reticulocyte volume (B) reticulocyte percentage (C) high light scatter reticulocyte percentage, (D) mean corpuscular hemoglobin concentration. Sample sizes are shown at top. 95% confidence intervals around group means are shown.

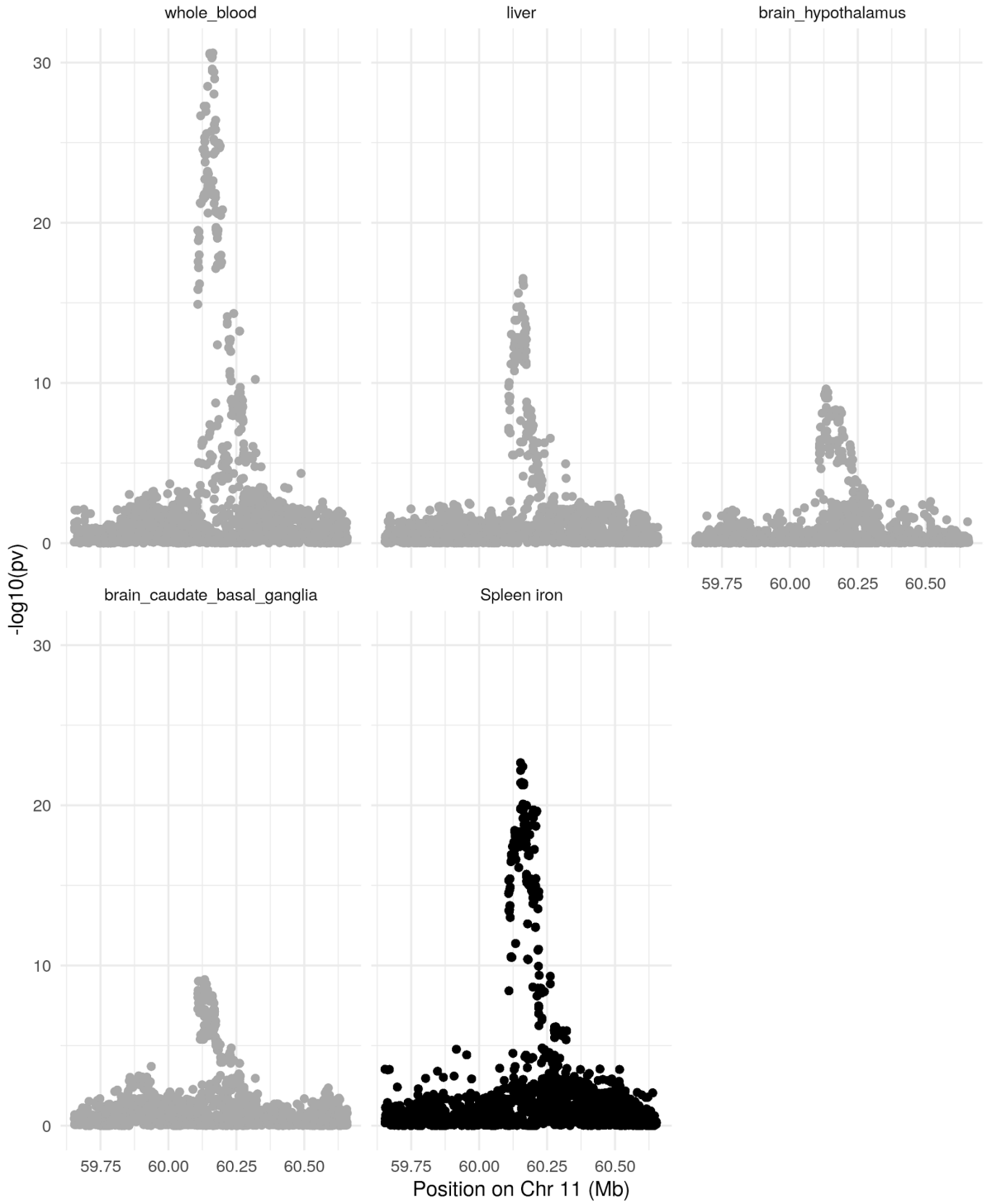

Supplementary Figure 11: Colocalization of spleen iron and expression of *MS4A14* in various tissues. Tissues are ordered by the strength of the colocalization.

References

1. Sun BB, Maranville JC, Peters JE, et al. Genomic atlas of the human plasma proteome. *Nature*. 2018;558(7708):73–79.
2. Sinnott-Armstrong N, Tanigawa Y, Amar D, et al. Genetics of 35 blood and urine biomarkers in the UK Biobank. *Nat. Genet.* 2021;53(2):185–194.
3. Liu DJ, Peloso GM, Yu H, et al. Exome-wide association study of plasma lipids in >300,000 individuals. *Nat. Genet.* 2017;49(12):1758–1766.
4. Littlejohns TJ, Holliday J, Gibson LM, et al. The UK Biobank imaging enhancement of 100,000 participants: rationale, data collection, management and future directions. *Nat. Commun.* 2020;11(1):2624.
5. Liu Y, Basty N, Whitcher B, et al. Genetic architecture of 11 organ traits derived from abdominal MRI using deep learning. *eLife*. 2021;10.:
6. Martin S, Cule M, Basty N, et al. Genetic Evidence for Different Adiposity Phenotypes and Their Opposing Influences on Ectopic Fat and Risk of Cardiometabolic Disease. *Diabetes*. 2021;70(8):1843–1856.
7. Schwenzer NF, Machann J, Haap MM, et al. T2* relaxometry in liver, pancreas, and spleen in a healthy cohort of one hundred twenty-nine subjects-correlation with age, gender, and serum ferritin. *Invest. Radiol.* 2008;43(12):854–860.
8. Angelucci E, Giovagnoni A, Valeri G, et al. Limitations of magnetic resonance imaging in measurement of hepatic iron. *Blood*. 1997;90(12):4736–4742.
9. Saito H. METABOLISM OF IRON STORES. *Nagoya J. Med. Sci.* 2014;76(3-4):235–254.
10. Kolnagou A, Michaelides Y, Kontoghiorghe CN, Kontoghiorghes GJ. The importance of spleen, spleen iron, and splenectomy for determining total body iron load, ferrikinetics, and iron toxicity in thalassemia major patients. *Toxicol. Mech. Methods*. 2013;23(1):34–41.
11. Brewer CJ, Coates TD, Wood JC. Spleen R2 and R2* in iron-overloaded patients with sickle cell disease and thalassemia major. *J. Magn. Reson. Imaging*. 2009;29(2):357–364.
12. Papakonstantinou O, Alexopoulou E, Economopoulos N, et al. Assessment of iron distribution between liver, spleen, pancreas, bone marrow, and myocardium by means of R2 relaxometry with MRI in patients with beta-thalassemia major. *J. Magn. Reson. Imaging*. 2009;29(4):853–859.
13. Aslan E, Luo JW, Lesage A, et al. MRI-based R2* mapping in patients with suspected or known iron overload. *Abdom Radiol (NY)*. 2021;
14. Çetinçakmak MG, Hattapoğlu S, Söker M, et al. Evaluation of the relationship between splenic iron overload and liver, heart and muscle features evident on T2*-weighted magnetic resonance imaging. *Adv. Clin. Exp. Med.* 2020;29(4):475–480.
15. Adler DD, Glazer GM, Aisen AM. MRI of the spleen: normal appearance and findings in sickle-cell anemia. *AJR Am. J. Roentgenol.* 1986;147(4):843–845.
16. França M, Martí-Bonmatí L, Porto G, et al. Tissue iron quantification in chronic liver diseases using MRI shows a relationship between iron accumulation in liver, spleen, and bone marrow. *Clin. Radiol.* 2018;73(2):215.e1–215.e9.
17. Adams P, Brissot P, Powell LW. EASL International Consensus Conference on Haemochromatosis. *J. Hepatol.* 2000;33(3):485–504.
18. Biro C, Kopani M, Kopaniova A, et al. Iron accumulation in human spleen in autoimmune thrombocytopenia and hereditary spherocytosis. *Bratisl. Lek. Listy*. 2012;113(2):92–94.
19. Deugnier Y, Bardou-Jacquet É, Lainé F. Dysmetabolic iron overload syndrome (DIOS). *Presse Med.* 2017;46(12 Pt 2):e306–e311.
20. Mendler MH, Turlin B, Moirand R, et al. Insulin resistance-associated hepatic iron overload. *Gastroenterology*. 1999;117(5):1155–1163.

21. Siegelman ES, Mitchell DG, Semelka RC. Abdominal iron deposition: metabolism, MR findings, and clinical importance. *Radiology*. 1996;199(1):13–22.
22. Yiannikourides A, Latunde-Dada G. A Short Review of Iron Metabolism and Pathophysiology of Iron Disorders. *Medicines*. 2019;6(3):85.
23. Ganz T. Systemic iron homeostasis. *Physiol. Rev.* 2013;93(4):1721–1741.
24. Dzierzak E, Philipsen S. Erythropoiesis: Development and Differentiation. *Cold Spring Harbor Perspectives in Medicine*. 2013;3(4):a011601–a011601.
25. Gallagher PG. Red cell membrane disorders. *Hematology Am. Soc. Hematol. Educ. Program*. 2005;13–18.
26. Delaunay J. Molecular basis of red cell membrane disorders. *Acta Haematol.* 2002;108(4):210–218.
27. Bennett V, Baines AJ. Spectrin and ankyrin-based pathways: metazoan inventions for integrating cells into tissues. *Physiol. Rev.* 2001;81(3):1353–1392.
28. Ovchynnikova E, Aglialoro F, von Lindern M, van den Akker E. The Shape Shifting Story of Reticulocyte Maturation. *Frontiers in Physiology*. 2018;9.:
29. Klei T, Van Bruggen R, Dalimot J, et al. Hemolysis in the Spleen Drives Erythrocyte Turnover. *Blood*. 2019;134(Supplement_1):946–946.
30. Arora RD, Dass J, Maydeo S, et al. Utility of mean sphered cell volume and mean reticulocyte volume for the diagnosis of hereditary spherocytosis. *Hematology*. 2018;23(7):413–416.
31. van Vuren A, van der Zwaag B, Huisjes R, et al. The Complexity of Genotype-Phenotype Correlations in Hereditary Spherocytosis: A Cohort of 95 Patients. *HemaSphere*. 2019;3(4):e276.
32. Chonat S, Risinger M, Sakthivel H, et al. The Spectrum of SPTA1-Associated Hereditary Spherocytosis. *Frontiers in Physiology*. 2019;10.:
33. Tole S, Dhir P, Pugi J, et al. Genotype–phenotype correlation in children with hereditary spherocytosis. *British Journal of Haematology*. 2020;191(3):486–496.
34. Bycroft C, Freeman C, Petkova D, et al. The UK Biobank resource with deep phenotyping and genomic data. *Nature*. 2018;562(7726):203–209.
35. Henninger B, Alustiza J, Garbowski M, Gandon Y. Practical guide to quantification of hepatic iron with MRI. *Eur. Radiol.* 2020;30(1):383–393.
36. Elliott LT, Sharp K, Alfaro-Almagro F, et al. Genome-wide association studies of brain imaging phenotypes in UK Biobank. *Nature*. 2018;562(7726):210–216.
37. Bell S, Rigas AS, Magnusson MK, et al. A genome-wide meta-analysis yields 46 new loci associating with biomarkers of iron homeostasis. *Commun Biol*. 2021;4(1):156.
38. Consortium TG, The GTEx Consortium. The GTEx Consortium atlas of genetic regulatory effects across human tissues. *Science*. 2020;369(6509):1318–1330.
39. Chen M-H, Raffield LM, Mousas A, et al. Trans-ethnic and Ancestry-Specific Blood-Cell Genetics in 746,667 Individuals from 5 Global Populations. *Cell*. 2020;182(5):1198–1213.e14.
40. Uhlen M, Karlsson MJ, Zhong W, et al. A genome-wide transcriptomic analysis of protein-coding genes in human blood cells. *Science*. 2019;366(6472.):
41. Anderson LJ, Holden S, Davis B, et al. Cardiovascular T2-star (T2*) magnetic resonance for the early diagnosis of myocardial iron overload. *Eur. Heart J.* 2001;22(23):2171–2179.
42. Sirlin CB, Reeder SB. Magnetic resonance imaging quantification of liver iron. *Magn. Reson. Imaging Clin. N. Am.* 2010;18(3):359–81, ix.
43. Fernandes JL. MRI for Iron Overload in Thalassemia. *Hematol. Oncol. Clin. North Am.* 2018;32(2):277–295.
44. Arrivé L, Thurnher S, Hricak H, Price DC. Magnetic resonance imaging of splenic iron overload. *Eur. J. Radiol.* 1990;10(2):98–104.
45. Ooi GC, Chen FE, Chan KN, et al. Qualitative and quantitative magnetic resonance imaging in haemoglobin H disease: screening for iron overload. *Clin. Radiol.* 1999;54(2):98–102.

46. Rushton DH, Barth JH. What is the evidence for gender differences in ferritin and haemoglobin? *Crit. Rev. Oncol. Hematol.* 2010;73(1):1–9.
47. Timmers PRHJ, Wilson JF, Joshi PK, Deelen J. Multivariate genomic scan implicates novel loci and haem metabolism in human ageing. *Nat. Commun.* 2020;11(1):3570.
48. McKay A, Wilman HR, Dennis A, et al. Measurement of liver iron by magnetic resonance imaging in the UK Biobank population. *PLoS One*. 2018;13(12):e0209340.
49. Harrison-Findik DD. Role of alcohol in the regulation of iron metabolism. *World Journal of Gastroenterology*. 2007;13(37):4925.
50. Labranche R, Gilbert G, Cerny M, et al. Liver Iron Quantification with MR Imaging: A Primer for Radiologists. *Radiographics*. 2018;38(2):392–412.
51. Gutiérrez L, House MJ, Vasavda N, et al. Tissue Iron Distribution Assessed by MRI in Patients with Iron Loading Anemias. *PLoS One*. 2015;10(9):e0139220.
52. Pietrangelo A. Ferroportin disease: pathogenesis, diagnosis and treatment. *Haematologica*. 2017;102(12):1972–1984.
53. Silva-Gomes R, Mapelli SN, Boutet M-A, et al. Differential expression and regulation of MS4A family members in myeloid cells in physiological and pathological conditions. *J. Leukoc. Biol.* 2021;
54. Kuek LE, Leffler M, Mackay GA, Hulett MD. The MS4A family: counting past 1, 2 and 3. *Immunology & Cell Biology*. 2016;94(1):11–23.
55. Swirski FK, Nahrendorf M, Etzrodt M, et al. Identification of splenic reservoir monocytes and their deployment to inflammatory sites. *Science*. 2009;325(5940):612–616.
56. Reeder SB, Pineda AR, Wen Z, et al. Iterative decomposition of water and fat with echo asymmetry and least-squares estimation (IDEAL): Application with fast spin-echo imaging. *Magnetic Resonance in Medicine*. 2005;54(3):636–644.
57. Basty N, Liu Y, Cule M, et al. Automated Measurement of Pancreatic Fat and Iron Concentration Using Multi-Echo and T1-Weighted MRI Data. *2020 IEEE 17th International Symposium on Biomedical Imaging (ISBI)*. 2020;
58. Wood JC, Enriquez C, Ghugre N, et al. MRI R2 and R2* mapping accurately estimates hepatic iron concentration in transfusion-dependent thalassemia and sickle cell disease patients. *Blood*. 2005;106(4):1460–1465.
59. Hong CW, Hamilton G, Hooker C, et al. Measurement of spleen fat on MRI-proton density fat fraction arises from reconstruction of noise. *Abdom Radiol (NY)*. 2019;44(10):3295–3303.
60. Karczewski KJ, Francioli LC, Tiao G, et al. The mutational constraint spectrum quantified from variation in 141,456 humans. *Nature*. 2020;581(7809):434–443.
61. Kircher M, Witten DM, Jain P, et al. A general framework for estimating the relative pathogenicity of human genetic variants. *Nat. Genet.* 2014;46(3):310–315.
62. Zhou W, Zhao Z, Nielsen JB, et al. Scalable generalized linear mixed model for region-based association tests in large biobanks and cohorts. *Nat. Genet.* 2020;52(6):634–639.
63. Sethi A, Taylor L, Graham Ruby J, et al. Calcification of abdominal aorta is an underappreciated cardiovascular disease risk factor.
64. Loh P-R, Tucker G, Bulik-Sullivan BK, et al. Efficient Bayesian mixed-model analysis increases association power in large cohorts. *Nat. Genet.* 2015;47(3):284–290.
65. Yang J, Benyamin B, McEvoy BP, et al. Common SNPs explain a large proportion of heritability for human height. *Nat. Genet.* 2010;42(7):565.
66. Bulik-Sullivan BK, Finucane HK, Anttila V, et al. An atlas of genetic correlations across human diseases and traits. *Nat. Genet.* 2015;47(11):1236–1241.
67. Yang J, Ferreira T, Morris AP, et al. Conditional and joint multiple-SNP analysis of GWAS summary statistics identifies additional variants influencing complex traits. *Nat. Genet.* 2012;44(4):369–75, S1–3.
68. GTEx Consortium, Laboratory, Data Analysis &Coordinating Center (LDACC)—Analysis Working Group, Statistical Methods groups—Analysis Working Group, et al. Genetic effects on gene expression across human tissues. *Nature*. 2017;550(7675):204–213.
69. Zhou W, Nielsen JB, Fritsche LG, et al. Efficiently controlling for case-control imbalance

and sample relatedness in large-scale genetic association studies. *Nat. Genet.* 2018;50(9):1335–1341.
70. Giambartolomei C, Vukcevic D, Schadt EE, et al. Bayesian test for colocalisation between pairs of genetic association studies using summary statistics. *PLoS Genet.* 2014;10(5):e1004383.
71. Guo H, Fortune MD, Burren OS, et al. Integration of disease association and eQTL data using a Bayesian colocalisation approach highlights six candidate causal genes in immune-mediated diseases. *Hum. Mol. Genet.* 2015;24(12):3305–3313.
72. Carroll RJ, Bastarache L, Denny JC. R PheWAS: data analysis and plotting tools for phenome-wide association studies in the R environment. *Bioinformatics*. 2014;30(16):2375–2376.
73. Millard LAC, Davies NM, Gaunt TR, Davey Smith G, Tilling K. Software Application Profile: PHESANT: a tool for performing automated phenome scans in UK Biobank. *Int. J. Epidemiol.* 2018;47(1):29–35.
74. Regier AA, Farjoun Y, Larson DE, et al. Functional equivalence of genome sequencing analysis pipelines enables harmonized variant calling across human genetics projects. *Nat. Commun.* 2018;9(1):4038.
75. St Pierre TG, Clark PR, Chua-anusorn W, et al. Noninvasive measurement and imaging of liver iron concentrations using proton magnetic resonance. *Blood*. 2005;105(2):855–861.